

Seasonal variability of nitrous oxide concentrations and emissions in a temperate estuary

Gesa Schulz^{1,2}, Tina Sanders², Yoana G. Voynova², Hermann W. Bange³, and Kirstin Dähnke²

¹Institute of Geology, Center for Earth System Research and Sustainability (CEN), University Hamburg, Hamburg, 20146, Germany

²Institute of Carbon Cycles, Helmholtz Centre Hereon, Geesthacht, 21502, Germany

³Marine Biogeochemistry Research Division, GEOMAR Helmholtz Centre for Ocean Research Kiel, Kiel, 24105, Germany

Correspondence to: Gesa Schulz (Gesa.Schulz@hereon.de)

Abstract

Nitrous oxide (N₂O) is a greenhouse gas, with a global warming potential 298 times that of carbon dioxide. Estuaries can be sources of N₂O, but their emission estimates have significant uncertainties due to limited data availability and high spatiotemporal variability. We investigated the spatial and seasonal variability of dissolved N₂O and its emissions along the Elbe Estuary (Germany), a well-mixed temperate estuary with high nutrient loading from agriculture. During nine research cruises performed between 2017 and 2022, we measured dissolved N₂O concentrations, as well as dissolved nutrients and oxygen concentrations along the estuary and calculated N₂O saturations, flux densities and emissions. We found that the estuary was a year-round source of N₂O, with highest emissions in winter when dissolved inorganic nitrogen (DIN) loads and wind speeds are high. However, in spring and summer, N₂O saturations and emissions did not decrease alongside lower riverine nitrogen loads, suggesting that estuarine in-situ N₂O production is an important source of N₂O. We identified two hot-spots areas of N₂O production: the Port of Hamburg, a major port region, and the mesohaline estuary near the maximum turbidity zone (MTZ). N₂O production was ~~enhanced by warmer temperatures and was~~ fueled by decomposition of riverine organic matter in the Hamburg Port and by marine organic matter in the MTZ. A comparison with previous measurements in the Elbe Estuary revealed that N₂O saturation did not decrease alongside ~~with the decrease in~~ DIN concentrations after a significant improvement of water quality in the 1990s that allowed for phytoplankton growth to reestablish in the river and estuary. ~~Theis effect-overarching control~~ of phytoplankton growth ~~and the overarching control of on~~ organic matter ~~and, subsequently, on~~ N₂O production, highlights ~~the fact~~ that eutrophication and ~~elevated~~ agricultural nutrient input can increase N₂O emissions in estuaries.

1 Introduction

Nitrous oxide (N₂O) is an important atmospheric trace gas that contributes to global warming and stratospheric ozone depletion (WMO, 2018; IPCC, 2021). Estuaries are important regions of nitrogen turnover (Middelburg and Nieuwenhuize, 2000; Crossland et al., 2005; Bouwman et al., 2013), and a potential source of N₂O (Bange, 2006; Barnes and Upstill-Goddard, 2011; Murray et al., 2015). Together with coastal wetlands, estuaries contribute between 0.17 and 0.95 Tg N₂O-N of the annual global budget of 16.9 Tg N₂O-N (Murray et al., 2015; Tian et al., 2020). N₂O emission estimates from estuaries are associated with significant uncertainties due to limited data availability and high spatiotemporal variability (e.g. Bange, 2006; Barnes and Upstill-Goddard, 2011; Maavara et al., 2019), presenting a big challenge for the global N₂O emission estimates.

39 Nitrification and denitrification are the most important N₂O production pathways in estuaries. Under oxic
40 conditions, N₂O is produced as a side product during the first step of nitrification, the oxidation of ammonia to
41 nitrite (e.g. Wrage et al., 2001; Barnes and Upstill-Goddard, 2011). At low oxygen (but not anoxic) conditions,
42 nitrifier-denitrification may occur, during which nitrifiers reduce nitrite to N₂O (e.g. Wrage et al., 2001; Bange,
43 2008). Denitrification takes place under anoxic conditions and mostly acts as a source of N₂O, but can also reduce
44 N₂O to N₂ (e.g. Knowles, 1982; Bange, 2008). In estuaries, denitrification can occur in anoxic sediments, the
45 anoxic water column or anoxic microsites of particles, whereas nitrification and nitrifier-denitrification take place
46 in the oxygenated water column (Beaulieu et al., 2010; Murray et al., 2015; Ji et al., 2018; Tang et al., 2022).

47 In estuaries, the most important factors controlling N₂O emissions are considered to be oxygen availability and
48 dissolved inorganic nitrogen loads (Murray et al., 2015). Since N₂O measurements in estuaries are scarce, global
49 N₂O emissions can be estimated by using emission factors and considering dissolved inorganic nitrogen (DIN) or
50 total nitrogen (TN) loads, where it is assumed that higher [nitrogen](#) loads lead to higher N₂O emissions (Kroeze et
51 al., 2005, 2010; Ivens et al., 2011; Hu et al., 2016). However, several studies instead reported no obvious
52 relationship between nitrogen concentrations and N₂O emissions (Borges et al., 2015; Marzadri et al., 2017; Wells
53 et al., 2018), highlighting the need to understand the causes for variability ~~in~~ the relationship between nitrogen
54 loads and N₂O emissions (Wells et al., 2018).

55 The Elbe Estuary is a heavily managed estuary with high agricultural nitrogen inputs that hosts the third largest
56 port in Europe (e.g. Radach and Pätsch, 2007; Bergemann and Gaumert, 2008; Pätsch et al., 2010; Quiel et al.,
57 2011). It has been identified as a N₂O source, with a hotspot of N₂O production in the Port of Hamburg (Hanke
58 and Knauth, 1990; Brase et al., 2017). We aimed to investigate drivers for N₂O emissions along the estuary,
59 specifically the N₂O and DIN ratio (N₂O:DIN). To do so, we (1) looked for potential long-term changes in N₂O
60 saturations, (2) investigated potential production hotspots, as well as the spatial and temporal distribution of N₂O
61 saturations, and (3) used the N₂O:DIN ratio for a comparison with other estuaries ~~that receive similar high~~
62 [agricultural nutrient inputs](#).

63 2 Methods

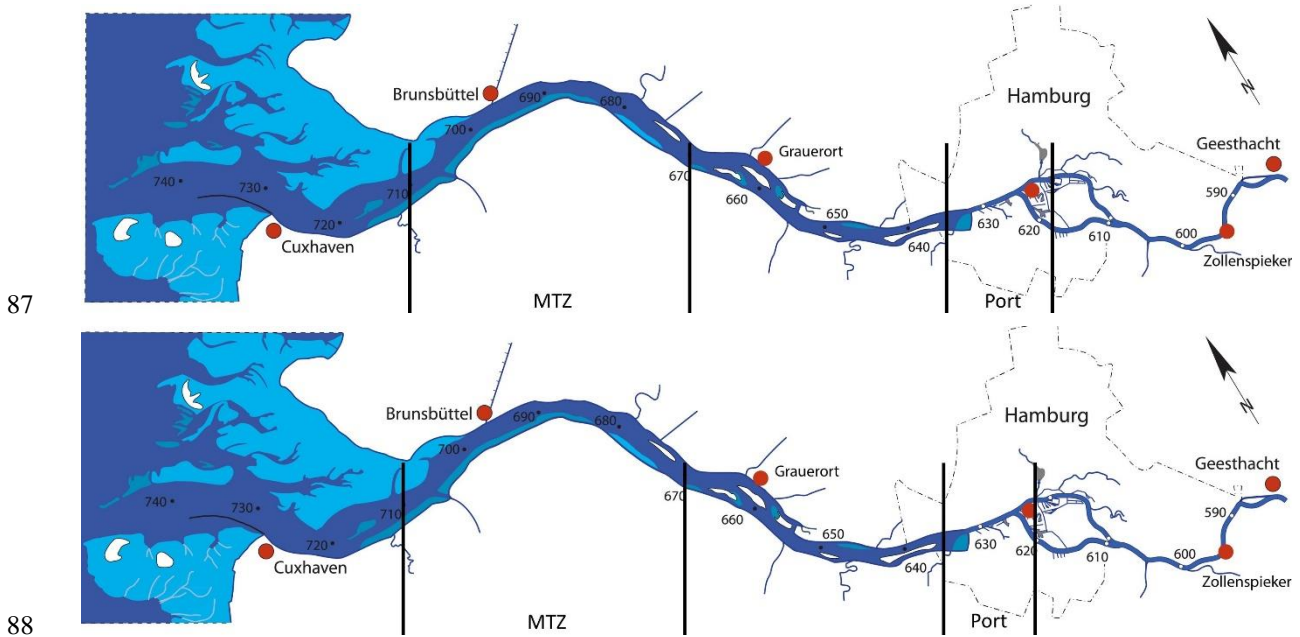
64 2.1 Study site

65 The Elbe River stretches over 1094 km from the Giant Mountains (Czech Republic) to the North Sea (Cuxhaven,
66 Germany). The catchment of the Elbe River is 140 268 km² (Boehlich and Strotmann, 2019), with 74 % urban and
67 agricultural land-use (Johannsen et al., 2008). The Elbe is the second largest German river discharging into the
68 North Sea, as well as the largest source of dissolved nitrogen for the German Bight, which is heavily affected by
69 eutrophication (van Beusekom et al., 2019).

70 The Elbe Estuary is a well-mixed temperate estuary, which begins at stream kilometer 586 at a weir in Geesthacht
71 and stretches through the Port of Hamburg, entering the North Sea near Cuxhaven at stream kilometer 727 (Fig.
72 1). Estuaries are commonly structured along their salinity gradient into an oligohaline (salinity: 0.5 – 5.0), a
73 mesohaline (salinity: 5.0 – 18.0) and a polyhaline (salinity > 18.0) [region](#) (US EPA, 2006). The Elbe Estuary has
74 a length of 142 km (Boehlich and Strotmann, 2019) and a mean annual discharge of 712 m³ s⁻¹ (measured at gauge
75 Neu Darchau at stream kilometer 536; HPA and Freie und Hansestadt Hamburg, 2017). The average water
76 residence time is ~32 days, ranging from ~72 days during times of low discharge (300 m³ s⁻¹) to ~10 days during
77 times of high discharge (2000 m³ s⁻¹; Boehlich and Strotmann, 2008). The [Elbe Estuary](#) has an annual nitrogen

78 load of 84 Gg-N (FGG Elbe, 2018), and point sources along the estuary provide only a small part of the total
79 nitrogen input to the Elbe Estuary (Hofmann et al., 2005; IKSE, 2018). Oxygen concentrations in the Elbe Estuary
80 vary seasonally, with oxygen depletion during the summer months and oxygen minimum zones regularly
81 experiencing concentrations below $94 \mu\text{mol O}_2 \text{ L}^{-1}$ (Schroeder, 1997; Gaumert and Bergemann, 2007; Schöl et al.,
82 2014).

83 The Elbe Estuary is dredged year-round to maintain a water depth of 15 – 20 m and to grant access for large
84 container ships to the Port of Hamburg (Boehlich and Strotmann, 2019; Hein et al., 2021). Construction work for
85 further deepening of the fairway was carried out during our study period, from 2019 to early 2022. Upstream of
86 the Port of Hamburg water depth is less than 10 m (Hein et al., 2021).



89 **Figure 1: Map of the Elbe Estuary sampled during our research cruises with stream kilometers (graphic courtesy of**
90 **FGG Elbe, modified after (Amann et al., 2012)). The light blue color indicates Wadden Sea areas that are exposed at**
91 **low tide. The vertical black lines indicate the Hamburg Port region and a typical position for the maximum turbidity**
92 **zone (MTZ, Bergemann, 2004).**

93 2.2 Transect sampling and measurements

94 We performed nine sampling campaigns along the estuary with the research vessel *Ludwig Prandtl* (Table 1). Most
95 cruises took place during spring and summer, with water temperatures $> 10 \text{ }^\circ\text{C}$ (May to September). Two cruises
96 were conducted during winter (early March, water temperature $< 6 \text{ }^\circ\text{C}$; Table 1). Transects started in the German
97 Bight, and continued along the salinity gradient, through the Port of Hamburg to Oortkaten (stream kilometer
98 609). To ensure comparable current and mixing conditions, transect sampling was always done after high-tide,
99 with the ship travelling upstream against the tide. For comparison to previous measurements, we included summer
100 data from a previous study in 2015 (Brase et al., 2017).

101 **Table 1: Campaign dates with the sampled Elbe Estuary sections shown via stream kilometers, average discharge**
 102 **during each cruise measured at the Neu Darchau gauging station, averages and standard deviations for water**
 103 **temperature, wind speed at 10 m height, dissolved inorganic nitrogen (DIN) concentrations for each campaign.**

Campaign Dates	Stream kilometers (km)	Water temperature (°C)	Wind speed 10 m (m s ⁻¹)	Average discharge (m ³ s ⁻¹)	Average DIN load concentrations (μmol L ⁻¹)
28.-29.04.2015	627 – 741	12.3 ± 1.0	7.4 ± 2.3	595	191.0 ± 45.0
02.-04.06.2015	609 – 739	17.4 ± 1.7	5.0 ± 1.3	276	105.9 ± 36.2
01.-02.08.2017	621 – 749	20.9 ± 0.7	3.6 ± 1.5	607	79.2 ± 30.2
04.-05.06.2019	610 – 750	18.7 ± 2.2	4.0 ± 1.7	423	108.3 ± 35.9
30.07.-01.08.2019	609 – 752	22.6 ± 1.0	4.2 ± 1.4	171	60.8 ± 38.6
19.-20.06.2020	609 – 747	19.8 ± 1.4	5.8 ± 1.2	331	74.6 ± 33.8
09.-11.09.2020	607 – 745	18.9 ± 0.6	5.9 ± 2.8	305	93.1 ± 32.7
10.-12.03.2021	609 – 748	5.4 ± 0.5	9.3 ± 2.6	862	324.4 ± 83.8
04.-05.05.2021	610 – 751	10.5 ± 0.8	11.0 ± 3.1	411	85.7 ± 36.6
27.-28.07.2021	621 – 751	22.2 ± 0.7	5.2 ± 1.3	721	139.8 ± 58.4
01.-02.03.2022	610 – 752	5.6 ± 0.2	2.9 ± 1.0	1282	238.0 ± 74.7

104 An onboard membrane pump continuously provided water at 1.2 m depth to an on-line in-situ FerryBox system
 105 and to an equilibrator used for the measurements of N₂O dry mole fraction (Section 2.4). The FerryBox system
 106 continuously measured water temperature, salinity, oxygen concentrations, pH and turbidity. We corrected the
 107 salinity corrected optode measurements using comparisons to Winkler titrations of ~~distinct~~-discrete samples. See
 108 Table S1 for further details.

109 Discrete water samples (30-40 samples for each cruise) were collected every 20 min from a bypass of the FerryBox
 110 system. For nutrient analysis, water samples were filtered immediately through combusted, pre-weighted GF/F
 111 Filters (4 h, 450 °C), and were frozen in acid washed PE-bottles until analysis. The filters were also stored frozen
 112 (-20 °C) and subsequently analyzed for suspended particulate matter (SPM), particulate nitrogen (PN), particulate
 113 carbon (PC) and C/N ratios (Fig. S1).

114 2.3 Nutrient measurements

115 Filtered water samples were measured in triplicates with a continuous flow auto analyzer (AA3, SEAL Analytics)
 116 using standard colorimetric and fluorometric methods (Hansen and Koroleff, 1999) for dissolved nitrate (NO₃⁻),
 117 nitrite (NO₂⁻) and ammonium (NH₄⁺) concentrations. Detection limits were 0.05 μmol L⁻¹, 0.05 μmol L⁻¹, and
 118 0.07 μmol L⁻¹ for nitrate, nitrite and ammonium, respectively.

119 2.4 Equilibrator based N₂O measurements and calculations

120 Equilibrated dry mole fractions of N₂O were measured by an N₂O analyzer based on off-axis integrated cavity
 121 output (OA-ICOS) absorption spectroscopy (Model 914-0022, Los Gatos Res. Inc., San Jose, CA, USA), which
 122 was coupled with a sea-water/gas equilibrator using off-axis cavity output spectroscopy. Brase et al. (2017)
 123 described the set-up and instrument precision in detail. Twice a day, two standard gas mixtures of N₂O in synthetic

124 air (500.5 ppb \pm 5 % and 321.2 ppb \pm 3 %) were analyzed to validate our measurements. No drift was detected
125 during our cruises.

126 We calculated the dissolved N₂O concentrations in water with the Bunsen solubility function of Weiss and Price
127 (1980), using 1 min averages of the measured N₂O dry mole fraction (ppb). Temperature differences between the
128 sample inlet and the equilibrator were taken into account for the calculation of the final N₂O concentrations Rhee
129 et al. (2009). N₂O saturation ~~were~~was calculated based on N₂O concentrations in water (N₂O_{cw}) and the
130 atmospheric equilibration concentrations (N₂O_{eq}; Eq. 1). Atmospheric N₂O dry mole fractions were measured
131 before and after each transect cruises using an air duct from the deck of the research vessel.

$$s = 100 \times \frac{N_2O_{cw}}{N_2O_{eq}} \quad (1)$$

132 The gas transfer coefficients (*k*) were determined based on Borges et al. (2004, Eq. 3), Nightingale et al. (2000),
133 Wanninkhof (1992) and Clark et al. (1995), using the Schmidt number (*Sc*) and wind speeds (*u*₁₀) measured at
134 10 m height (Eq. 2). The Schmidt number was calculated as ratio of the kinematic viscosity in water (Siedler and
135 Peters, 1986) to the N₂O diffusivity in water (Rhee, 2000). Cruise wind speeds (Table 1) varied significantly from
136 average annual wind speeds of the two federal states, in which the Elbe Estuary is located (4.7 m s⁻¹, Schleswig-
137 Holstein u. Hamburg: Mittlere Windgeschwindigkeit (1986-2015)* | Norddeutscher Klimamonitor, 2023), and
138 also compared to seasonal average wind speeds determined for the stations Cuxhaven and Hamburg (Rosenhagen
139 et al., 2011). Thus, to estimate uncertainties due to varying wind conditions during our cruises, we used 1) the
140 *in-situ* wind speeds measured on board the *R/V Ludwig Prandtl* at 10 m height by a MaxiMet GMX600 (Gill
141 Instruments Limited, Hampshire, UK), 2) the average annual wind speed (Schleswig-Holstein u. Hamburg:
142 Mittlere Windgeschwindigkeit (1986-2015)* | Norddeutscher Klimamonitor, 2023), and 3) the seasonally
143 averaged wind speeds (Rosenhagen et al., 2011). The flux densities in the main text were calculated using Eq. 3
144 and the wind speeds measured on board the vessel. Results of the other calculations are listed in the supplementary
145 material (Table S2).

$$k = 0.24 \times (4.045 + 2.58u_{10}) \times \left(\frac{Sc}{600}\right)^{-0.5} \quad (2)$$

$$f = k \times (N_2O_{cw} - N_2O_{air}) \quad (3)$$

146 To estimate N₂O emissions, we separated the Elbe Estuary into five regions: limnic (stream kilometer 585 to 615),
147 Port of Hamburg (stream kilometer 615 to 632), oligohaline (stream kilometer 632 to 704), mesohaline (stream
148 kilometer 704 – 727) and polyhaline (stream kilometer 727 to 750), see Table S3. Respective areas were provided
149 by the German Federal Waterways Engineering and Research Institute (BAW, pers. Comm., Oritz, 2023) and
150 Geerts et al. (2012). In order to account for seasonality, cruises were defined as: winter (March), spring (April and
151 May), summer (June and July) and late summer/autumn (August and September). We then calculated daily N₂O
152 emissions per section and season. For upscaling, we used the calculated monthly emissions to estimate annual
153 emissions (winter: November to March, spring: April to May, summer: June to July and late summer/autumn:
154 August to October). To address uncertainties, we calculated N₂O emissions based on different parametrizations
155 and wind speeds as described above.

156 2.5 Excess N₂O and apparent oxygen utilization

157 The correlation between excess N₂O (N₂O_{xs}) and apparent oxygen utilization (*AOU*) can provide insights into N₂O
158 production (Nevison et al., 2003; Walter et al., 2004). We calculated N₂O_{xs} as the difference between the N₂O

159 concentration in water (N_2O_w) and the theoretical equilibrium concentration (N_2O_{eq}) (Eq. 4). AOU was determined
160 using Eq. 5, where O_2 is the measured dissolved oxygen concentration, and O_2' is the theoretical equilibrium
161 concentration between water and atmosphere calculated according to Weiss (1970).

$$N_2O_{xs} = N_2O_{cw} - N_2O_{eq} \quad (4)$$

$$AOU = O_2' - O_2 \quad (5)$$

162 A linear relationship between AOU and N_2O_{xs} is usually an indicator for [N₂O production from](#) nitrification
163 (Nevison et al., 2003; Walter et al., 2004).

164 2.6 Statistical analysis

165 All statistical analyses were done using R packages. The packages ggpubr v.0.6.0 (Kassambara, 2023) and stats
166 v.4.0.2 (The R Stats Package, Version 4.0.2, 2021) were used to calculate Pearson correlations (R) and p -values.

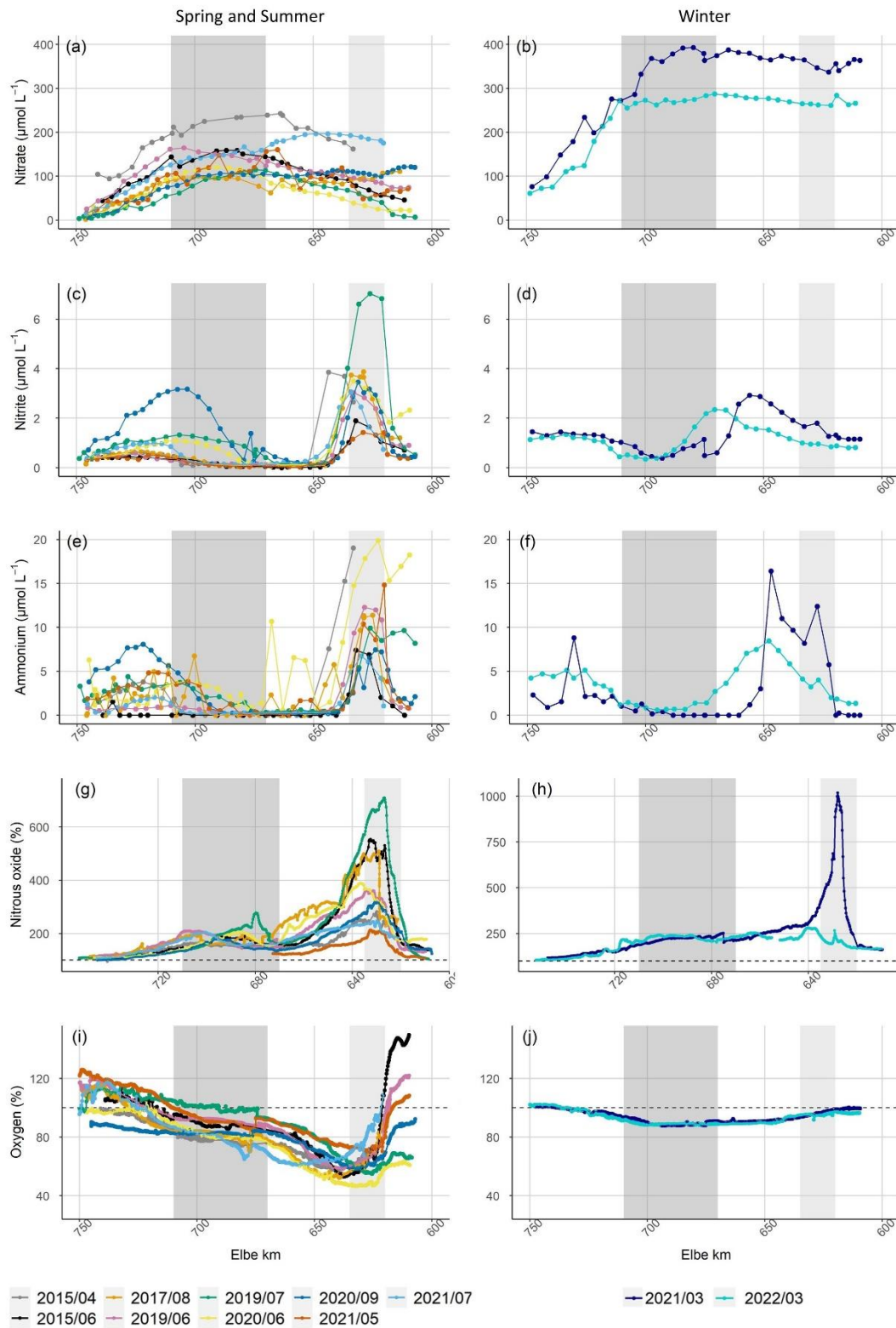
167 3 Results

168 3.1 Hydrographic properties and DIN distribution

169 Discharge ranged between $171 \text{ m}^3 \text{ s}^{-1}$ and $1282 \text{ m}^3 \text{ s}^{-1}$ during our cruises (ZDM, 2022), with higher discharge in
170 winter and lower discharge in summer (Table 1). Average water temperature over the entire estuary ranged from
171 $5.4 \pm 0.5 \text{ }^\circ\text{C}$ in March 2021 to $22.6 \pm 1.0 \text{ }^\circ\text{C}$ in August 2017 (Table 1). For further evaluation, March 2021 and
172 2022 cruises were regarded as winter cruises (water temperature $< 6^\circ\text{C}$), whereas all cruises with higher water
173 temperature were jointly regarded as spring and summer conditions.

174 Nitrate was the major form of dissolved inorganic nitrogen (DIN) during all cruises. In winter, high nitrogen
175 concentrations entered the estuary from the river. Towards summer, the riverine input of nitrate (stream kilometer
176 < 620) decreased, but along the estuary nitrate concentrations increased up to ~stream kilometer 700, then
177 decreased towards the North Sea. Nitrate concentrations were highest during both March cruises with averages of
178 $319.0 \pm 85.7 \text{ } \mu\text{mol L}^{-1}$ and $230.9 \pm 76.2 \text{ } \mu\text{mol L}^{-1}$ in 2021 and 2022, respectively. During summer, nitrate
179 concentrations were lower, with averages between $151.0 \pm 58.1 \text{ } \mu\text{mol L}^{-1}$ in May 2021 and $63.3 \pm 38.8 \text{ } \mu\text{mol L}^{-1}$
180 in July 2019 (Fig. 2a and b).

181 Nitrite and ammonium concentrations were usually low ($< 1 \text{ } \mu\text{mol L}^{-1}$) throughout the Elbe Estuary, but peaked
182 in the Hamburg Port region and around stream kilometer 720 (Fig. 2c and 2e). We measured pronounced variations
183 in nitrite concentrations during most of our cruises, ranging from $> 6.0 \text{ } \mu\text{mol L}^{-1}$ (July 2019) to concentrations
184 below the detection limit (Fig. 2c and d). The highest ammonium concentration was measured in March 2021 at
185 $23.5 \text{ } \mu\text{mol L}^{-1}$ (Fig. 2e and f).



186

187 **Figure 2: Nitrate concentration along the Elbe Estuary (a) in spring/summer, (b) in winter. Nitrite concentration along**
 188 **the Elbe Estuary (c) in spring/summer and (d) in winter. Ammonium concentration along the Elbe Estuary (e) in**
 189 **spring/summer and (f) in winter. N_2O in % saturation along the Elbe Estuary (g) in spring/summer, (h) in winter.**
 190 **Dissolved oxygen in % saturation along the Elbe Estuary (i) in spring/summer and (j) in winter. All variables are plotted**
 191 **against Elbe stream kilometers (Elbe km). Light grey shading denotes the Hamburg Port region, dark grey shading the**
 192 **typical position of the maximum turbidity zone (MTZ, Bergemann, 2004). Note the difference in Y-axis scales for the**
 193 **plots of (g) and (h). The dashed black lines in (g) and (h), as well as (i) and (j) indicate saturation of 100 % for nitrous**
 194 **oxide and dissolved oxygen, respectively.**

195 **3.2 Atmospheric N₂O and N₂O saturation**

196 The average atmospheric N₂O dry mole fractions ranged from 325 ppb in June 2015 to 336 ppb in July 2022 (Table
197 2). The differences between our measurements and the mean monthly N₂O mole fraction measured at the Mace
198 Head atmospheric monitoring station (Ireland; Dlugokencky et al., 2022) were always less than 1.5 %, indicating
199 a good agreement with the monitoring data.

200 During all cruises, the Elbe Estuary was supersaturated in N₂O in the freshwater region (Fig. 2g, h). The average
201 N₂O saturation over the entire transect ranged between 146 % and 243 % with an overall average of 197 % for all
202 cruises. Highest N₂O occurred in the Hamburg Port region in spring and summer with an average N₂O peak of
203 402 % saturation and a maximum supersaturation of 710 % in July 2019. The distributions of N₂O during winter
204 cruises were significantly different: In March 2022, highest N₂O (280 % saturation) occurred at stream kilometer
205 640. In contrast, in March 2021, we found an extraordinarily high peak with a saturation of 1018 % at stream
206 kilometer 627. Between stream kilometer 680 and 720, a supersaturation of up to 277 % occurred in spring and
207 summer. Further towards the North Sea, N₂O decreased, approaching equilibrium with the atmosphere.

208 **3.3 N₂O flux densities and N₂O emissions**

209 For N₂O flux densities, we ~~in the following~~ present calculated values after Borges et al. (2004, Table 2), ~~but also~~
210 ~~include results using other parametrizations in-~~ See Table S2 ~~and Fig. S2 for results of other parametrizations~~. The
211 N₂O flux densities were usually highest in the Hamburg Port area, with an average of $95.0 \pm 97.9 \mu\text{mol m}^{-2} \text{d}^{-1}$ and
212 lowest towards the North Sea, with an average of $3.9 \pm 3.0 \mu\text{mol m}^{-1} \text{d}^{-1}$ (Elbe stream kilometers > 735). The
213 average N₂O flux density of all cruises was $39.9 \pm 46.9 \mu\text{mol m}^{-2} \text{d}^{-1}$ (calculated with *in-situ* wind speeds measured
214 during the cruises).

215 **Table 2: Calculated average N₂O saturation, sea-to-air fluxes calculated following Borges et al. (2004) and atmospheric**
216 **N₂O dry mole fractions during our cruises in the Elbe Estuary**

Campaign Dates	Average saturation (%)	N ₂ O Flux densities ($\mu\text{mol m}^{-2} \text{d}^{-1}$)			Average atmospheric dry mole fraction (ppb)
		In-situ wind	Annual wind	Seasonal wind	
28.-29.04.15	160.8 ± 37.9	33.1 ± 21.0	23.1 ± 14.7	25.4 ± 16.1	331 ± 0.5
02.-04.06.15	203.8 ± 112.7	39.0 ± 42.7	37.2 ± 40.7	37.8 ± 41.4	325 ± 0.8
01.-02.08.17	221.0 ± 106.5	35.6 ± 31.8	43.2 ± 38.5	44.1 ± 39.3	331 ± 1.2
04.-05.06.19	192.6 ± 66.0	29.7 ± 21.5	33.5 ± 24.2	34.0 ± 24.6	332 ± 0.2
30.07.-01.08.19	232.5 ± 155.3	42.0 ± 50.1	45.7 ± 54.5	47.4 ± 56.4	327 ± 1.0
19.-20.06.20	193.9 ± 74.1	39.2 ± 31.6	33.3 ± 26.9	33.9 ± 27.3	330 ± 0.6
09.-11.09.20	160.5 ± 53.6	26.0 ± 23.5	21.8 ± 19.7	24.5 ± 22.1	331 ± 0.7
10.-12.03.21	242.5 ± 141.6	100.7 ± 101.2	58.1 ± 58.4	71.0 ± 71.4	331 ± 1.3
04.-05.05.21	145.6 ± 28.8	35.6 ± 22.5	17.8 ± 11.2	18.5 ± 11.7	331 ± 0.8
27.-28.07.21	172.6 ± 37.2	28.0 ± 14.6	25.9 ± 13.6	26.9 ± 14.1	334 ± 3.8
01.-02.03.22	196.5 ± 47.0	27.8 ± 13.9	39.0 ± 19.5	47.7 ± 23.8	333 ± 0.7

217
218 N₂O emission estimates varied significantly depending on the used parametrization and wind speeds. Note that we
219 calculated emissions twice: 1) including (w 03/2021) and 2) deliberately excluding (w/o 03/2021) the N₂O peak
220 saturation measured in the Port of Hamburg in March 2021, using ~~a-linearly~~ interpolated concentrations, ~~in the~~

221 [respectively](#). Highest emissions were calculated following methods by Borges et al. (2004) and using
 222 *in-situ* wind speeds, resulting in emissions of 0.25 ± 0.16 Gg-N₂O yr⁻¹ and 0.23 ± 0.12 Gg-N₂O yr⁻¹ with and
 223 without the N₂O peak in March 2021, respectively. Lowest emissions of 0.08 Gg-N₂O yr⁻¹ arose with
 224 parametrization of Nightingale et al. (2000) and Wanninkhof (1992), and using annual wind speeds (Table 3).

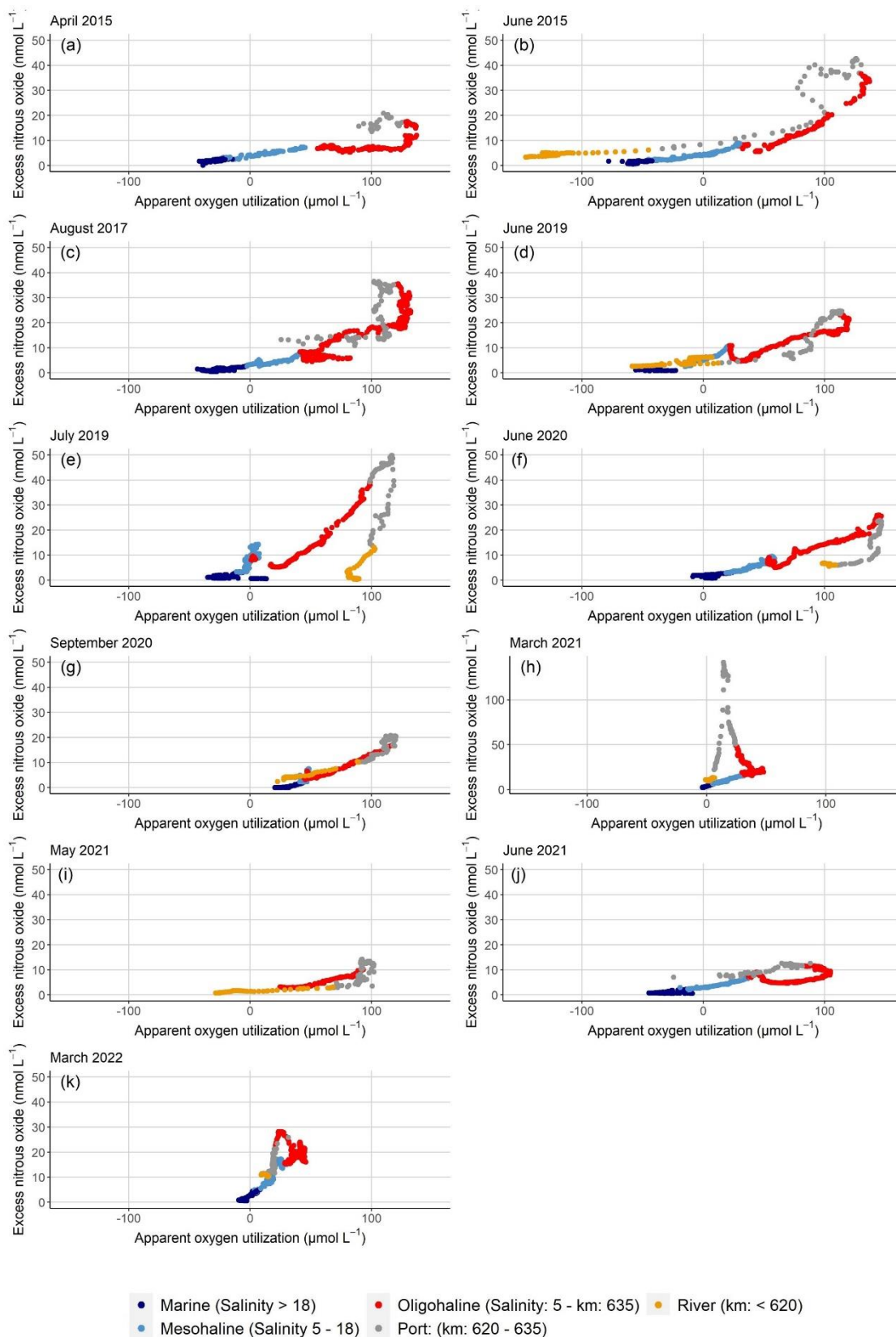
225 **Table 3: Annual N₂O emission estimates in Gg-N₂O yr⁻¹ calculated with different parametrizations and wind speeds**

		Emissions in Gg-N ₂ O yr ⁻¹			
		Borges et al. (2004)	Nightingale et al. (2000)	Wanninkhof (1992)	Clark et al. (1995)
w	In-situ wind	0.25 ± 0.16	0.14 ± 0.12	0.17 ± 0.15	0.16 ± 0.12
03/2021	Annual wind	0.21 ± 0.11	0.08 ± 0.04	0.09 ± 0.05	0.09 ± 0.05
	Seasonal wind	0.24 ± 0.12	0.11 ± 0.06	0.13 ± 0.06	0.12 ± 0.06
w/o	In-situ wind	0.23 ± 0.12	0.13 ± 0.09	0.15 ± 0.11	0.14 ± 0.09
03/2021	Annual wind	0.20 ± 0.08	0.08 ± 0.03	0.08 ± 0.03	0.09 ± 0.04
	Seasonal wind	0.22 ± 0.09	0.11 ± 0.04	0.12 ± 0.04	0.12 ± 0.04

226 3.4 Dissolved oxygen saturation

227 Average oxygen varied between 76 and 95 [in](#) % saturation with an oxygen minimum in the Hamburg Port area.
 228 Winter cruises varied little, with oxygen remaining relatively constant along the estuary (> 88 % saturation).
 229 During most spring and summer cruises, water from the river coming into the estuary was supersaturated in oxygen
 230 (> 100 % saturation). In the Hamburg Port region, oxygen saturation generally decreased. Lowest values occurred
 231 in June 2020 with 47 % saturation. The along-estuary oxygen minimum in summer months (June to August) was
 232 always below 61 % saturation. In spring and summer, oxygen increased towards the North Sea and reached
 233 100 % saturation (Fig. 2i and j).

234 Plots of excess N₂O (N₂O_{xs}) and apparent oxygen utilization (AOU) revealed excess N₂O along the entire estuary
 235 (Fig. 3). During all cruises, elevated riverine N₂O_{xs} entered the estuary (stream kilometer < 620). A linear positive
 236 relationship between N₂O_{xs} and AOI suggested nitrification as main production pathway in large sections of the
 237 estuary (Nevison et al., 2003; Walter et al., 2004). However, in summer, a change of slope in the Port of Hamburg
 238 as well as in the mesohaline section of the estuary suggested either increased *in-situ* N₂O production or external
 239 N₂O input. In winter, we found an increasing slope in the Hamburg Port region and in the oligohaline part of the
 240 Elbe Estuary (Fig. 3h, k).



241

242 **Figure 3: Plots of N_2O_{xs} vs AOU for (a) April 2015, (b) June 2015, (c) August 2017, (d) June 2019, (e) July 2019, (f) June**

243 **2020, (g) September 2020, (h) March 2021, (i) May 2021, (j) June 2021 and (k) March 2022. The values are colored to**

244 **distinguish between different regions of the estuary. Y-axis scale differ for Fig. 3h.**

245 3.5 Statistical analysis

246 We performed [a](#)-statistical analyses to identify potential N₂O production pathways and controlling factors. Table 4
 247 summarizes the results for the entire data set with further separation into spring and summer cruises (sp/su), as
 248 well as separation according to [the](#) presence of a salinity gradient (salinity > 1) or [of](#) freshwater regions (salinity
 249 < 1). Further[more](#), we performed corresponding analysis to assess the significance of correlations between for
 250 average values of different parameters for each cruise (Table 5). [N₂O saturation showed significant negative](#)
 251 [correlation with oxygen \(Table 4\) as well as a consistent negative correlation with pH \(Table 4 and 5\). Furthermore,](#)
 252 [nitrite concentrations positively correlated with N₂O saturation in the freshwater section of the estuary \(Table 4](#)
 253 [and 5\).](#)

254 **Table 4: Pearson correlation coefficients (R) for N₂O saturation (%) with temperature (T in °C), pH value, oxygen (O₂
 255 in % [saturation](#)), ammonium concentrations (NH₄⁺ in μmol L⁻¹), nitrite concentrations (NO₂⁻ in μmol L⁻¹), nitrate
 256 concentrations (NO₃⁻ in μmol L⁻¹), SPM concentrations (SPM in mg L⁻¹), C/N values, particulate carbon fraction (PC in
 257 %) and particulate nitrogen fraction (PN in %) for the entire data set, spring and summer cruises (sp/su), data with
 258 salinity > 1, spring and summer cruises with salinity > 1, data with salinity < 1 and spring and summer cruises with
 259 salinity < 1. The significance is shown as ** for p-value < 0.001, * for p-values < 0.01 and + for p-values < 0.05.**

N ₂ O saturation %	T °C	pH	O ₂ %	NH ₄ ⁺ μM	NO ₂ ⁻ μM	NO ₃ ⁻ μM	SPM mg	C/N	PC %	PN %
Entire data	0.06	-0.47**	-0.56**	0.27**	0.48**	0.23	0.10	0.60	-0.05	-0.13 ⁺
sp/su	0.33*	-0.59**	-0.65**	0.23**	0.53**	0.09	0.02	0.24**	-0.09	-0.13 ⁺
Sal>1	0.03	-0.40**	-0.53**	-0.32**	-0.05	0.71**	0.32**	0.11*	-0.24	-0.39**
Sal<1,	0.01	-0.41**	-0.42**	0.28**	0.51**	-0.00	-0.08	0.15	-0.25*	-0.24*
Sal>1, sp/su	-0.10	-0.21 ⁺	-0.52**	-0.28**	0.01	0.62**	0.02	0.39**	-0.31**	-0.41**
Sal<1, sp/su	0.30**	-0.60**	-0.57**	0.21 ⁺	0.58**	-0.23*	-0.16 ⁺	0.11	-0.30*	-0.27*

260

261 **Table 5: Pearson correlation coefficients (R) for average N₂O saturation (%) with average discharge (Q in m³ s⁻¹)
 262 temperature (T in °C), pH value, oxygen (O₂ in % [saturation](#)), ammonium concentrations (NH₄⁺ in μmol L⁻¹), nitrite
 263 concentrations (NO₂⁻ in μmol L⁻¹), nitrate concentrations (NO₃⁻ in μmol L⁻¹), SPM concentrations (SPM in mg L⁻¹), C/N
 264 values, particulate carbon fraction (PC in %) and particulate nitrogen fraction (PN in %) for the entire data set, spring
 265 and summer cruises (sp/su), data with salinity > 1, spring and summer cruises with salinity > 1, data with salinity < 1
 266 and spring and summer cruises with salinity < 1. The significance is shown as ** for p-value < 0.001, * for p-values <
 267 0.01 and + for p-values < 0.05.**

N ₂ O saturation %	Q m ³ s ⁻¹	T °C	pH	O ₂ %	NH ₄ ⁺ μM	NO ₂ ⁻ μM	NO ₃ ⁻ μM	SPM mg	C/N	PC %	PN %
Entire data	0.13	0.06	-0.65	-0.39	0.02	0.48	0.27	-0.31	0.53	0.12	-0.16
sp/su	-0.26	0.76 ⁺	-0.82 ⁺	-0.32	0.01	0.35	-0.40	-0.92*	0.15	0.18	0.31
Sal>1	-0.07	-0.14	-0.38	-0.43	-0.18	0.23	0.52	-0.19	0.46	-0.18	-0.38
Sal<1,	-0.21	0.29	-0.59	-0.39	0.26	0.76*	-0.11	-0.57	0.12	0.61	0.47
Sal>1, sp/su	-0.07	-0.70 ⁺	-0.41	-0.26	-0.42	0.03	0.05	-0.81 ⁺	-0.04	-0.10	0.14
Sal<1, sp/su	-0.48	0.72 ⁺	-0.80	-0.46	0.29	0.77 ⁺	-0.58	-0.87 ⁺	-0.17	0.69	0.67

268 4 Discussion

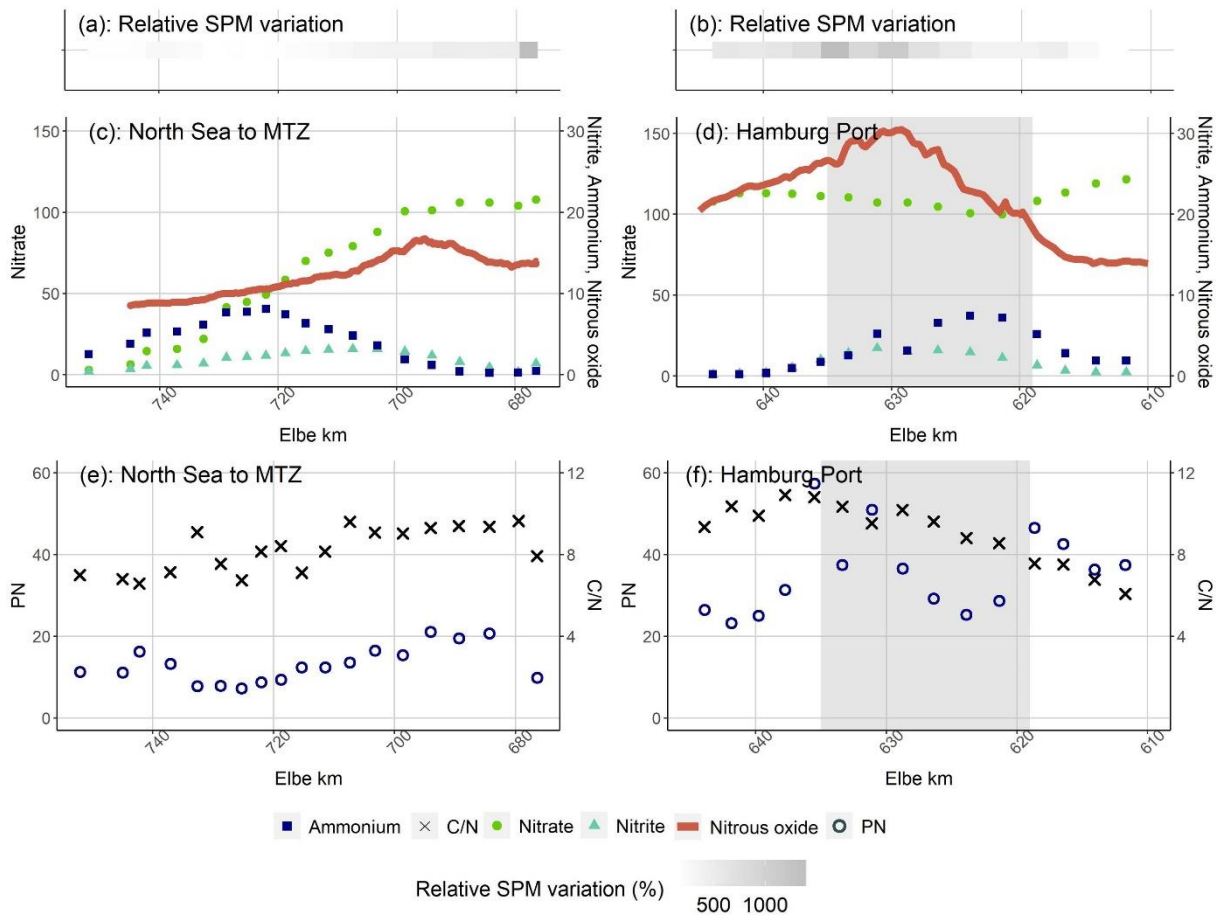
269 4.1 N₂O saturation and flux densities of the Elbe Estuary

270 The average N₂O saturation and flux density were 197 % and $39.9 \pm 46.9 \mu\text{mol m}^{-2} \text{d}^{-1}$, respectively. The N₂O flux
271 densities from the Elbe Estuary were in the mid-range of flux densities of other European estuaries ranging from
272 $2.9 \mu\text{mol m}^{-2} \text{d}^{-1}$ to $96.5 \mu\text{mol m}^{-2} \text{d}^{-1}$ (Garnier et al., 2006; Gonçalves et al., 2010; Murray et al., 2015) and average
273 N₂O saturations fitted to values determined by Reading et al. (2020) for highly modified urban systems. The
274 relationship of N₂O_{xs} and AOU (Fig. 3), with changing slopes in the Port of Hamburg and mesohaline estuary, was
275 determined by either initial riverine N₂O production, or in-situ production along the estuary. During spring and
276 summer, we found increasing N₂O concentrations in the Hamburg Port region (see also Brase et al. (2017)), and
277 in the salinity gradient (stream kilometer 680 – 700, salinity ~5). Both N₂O peaks varied in magnitude and spatial
278 extension, suggesting in-situ biological production (Fig. 2g). This matches earlier research linking estuarine N₂O
279 fluxes to in-situ generation (e.g. Bange, 2006; Barnes and Upstill-Goddard, 2011; Murray et al., 2015).

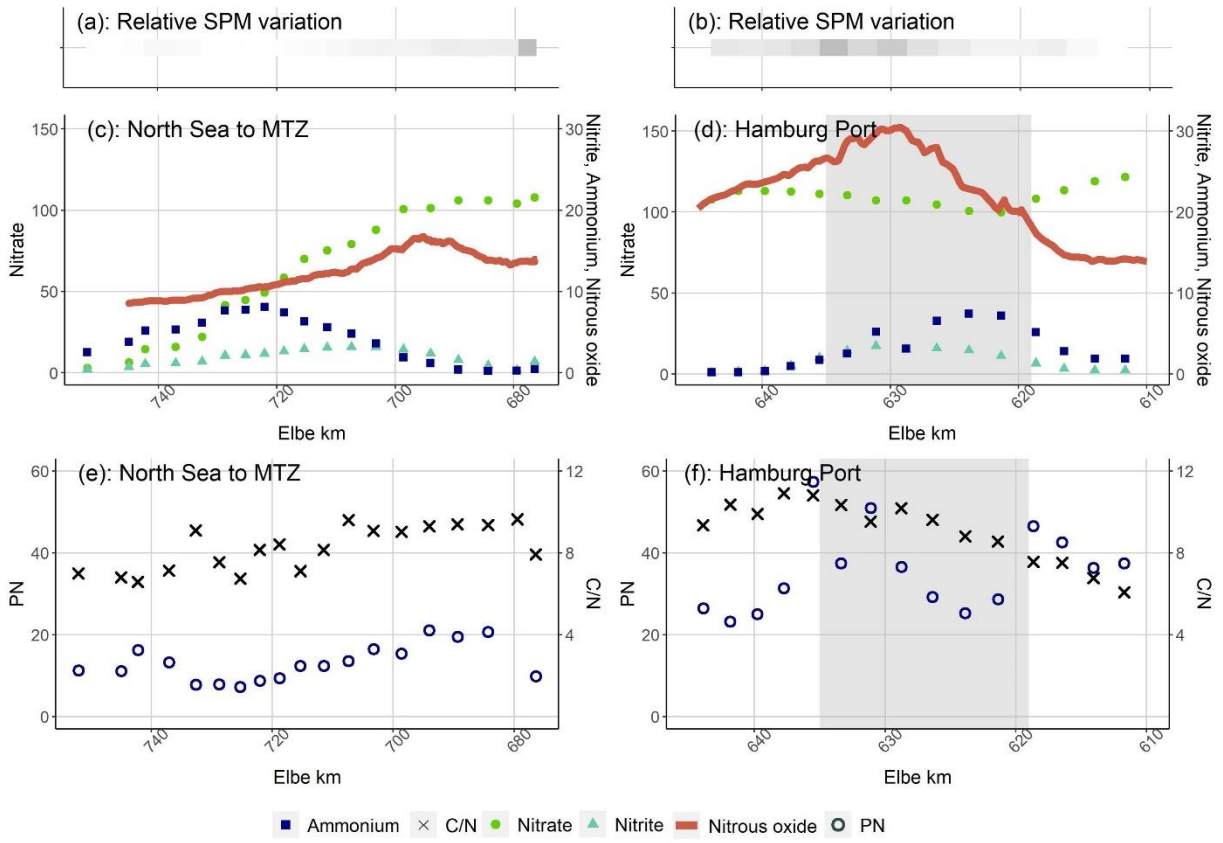
280 Previous measurements of N₂O saturation and flux densities in the Elbe Estuary between the 1980s and 2015
281 (Hanke and Knauth, 1990; Barnes and Upstill-Goddard, 2011; Brase et al., 2017) showed a significant reduction
282 of N₂O saturation due to the reduced riverine nutrient load and higher dissolved oxygen concentrations (Brase et
283 al., 2017). However, since the BIOGEST study in 1997 (Barnes and Upstill-Goddard, 2011), N₂O remained
284 relatively stable at ~ 200 % saturation despite a concurrent decrease in TN concentration from ~400 $\mu\text{mol L}^{-1}$ to
285 around 200 $\mu\text{mol L}^{-1}$ (Fig. [S2S3](#); Hanke and Knauth, 1990; Barnes and Upstill-Goddard, 2011; Brase et al., 2017;
286 Das Fachinformationssystem (FIS) der FGG Elbe, 2022). ~~Since~~ N₂O saturation did not decrease in scale with
287 riverine nitrogen input, this suggests that ~~the yield of N₂O production increased along the estuary. in-situ N₂O~~
288 ~~production along the estuary is important.~~ Dähnke et al. (2008) showed a shift from dominating denitrification
289 towards significant nitrification in the Elbe Estuary due to the significant improvement of water quality after the
290 reunification of Germany in 1990, ~~and this could influence N₂O distributions in the estuary.~~ In the following
291 sections, we investigate the biogeochemical controls of this in-situ N₂O production. For this purpose, we discuss
292 the two zones of intense N₂O production separately and also distinguish between cruises in spring and summer
293 (water temperature > 10 °C) and in winter (water temperature < 6 °C).

294 4.2 N₂O production in spring and summer in the mesohaline estuary

295 The N₂O peak in the transition between oligohaline and mesohaline estuary was accompanied by a sudden change
296 in the slope of the AOU vs N₂O_{xs} plots, (Fig. 3), pointing towards N₂O production in the oxic water column. Peaks
297 of nitrite and ammonium concentrations coincided with the elevated nitrous oxide saturations between Elbe km
298 680-700, with an ammonium peak around stream kilometer ~720, and a nitrite peak at ~700 (Fig. 4a). Highest
299 N₂O concentrations were usually measured between the nitrite peak and the region with highest turbidity (Fig. 4a,
300 September 2020, and Fig. [S3S4-S13S14](#)). This co-occurrence of nitrite accumulation and increased N₂O saturation
301 has been interpreted as signs for N₂O production via denitrification (e.g. Wertz et al., 2018; Sharma et al., 2022).
302 However, denitrification does not seem likely in this oxic water column. Such a succession of nitrite and
303 ammonium peaks is also typical for remineralization and nitrification, and the slight decrease of oxygen
304 concentrations around the higher N₂O saturation (Fig. 2g and i) suggests oxygen consumption, possibly caused by
305 these two processes. Sanders et al. (2018) measured small but detectable nitrification rates ($1 - 2 \mu\text{mol L}^{-1} \text{d}^{-1}$) for
306 this region of the Elbe Estuary, suggesting that N₂O may be a side product of nitrification.



307



308

309 **Figure 4: Succession of N-bearing substances coming from the North Sea and in the Port of Hamburg in September**
 310 **2020: Relative change of SPM concentrations (a) from the North Sea and (b) in the Port of Hamburg. Nitrate in**
 311 **$\mu\text{mol L}^{-1}$, nitrite in $\mu\text{mol L}^{-1}$, ammonium in $\mu\text{mol L}^{-1}$ and nitrous oxide concentrations in nmol L^{-1} plotted against Elbe**

312 stream kilometers (c) from the North Sea and (d) in the Port of Hamburg. Particulate nitrogen concentrations in
313 $\mu\text{mol L}^{-1}$ and C/N values plotted against stream kilometers (e) from the North Sea and (f) in the Port of Hamburg. The
314 grey area in (e) and (f) shows the position of the Port of Hamburg.

315 This [succession of N-bearing substances \(Fig. 4, Fig. S4-S14\)](#) suggests input of particulate matter from the North
316 Sea and upstream particle transport towards the maximum turbidity zone of the estuary (MTZ). This transport
317 mechanism is in line with Wolfstein and Kies (1999), who explained organic matter contents and chlorophyll a
318 concentrations in the polyhaline part of the Elbe Estuary by input of freshly produced particulate matter of marine
319 origin. Generally, maximum turbidity zones are generated by the balance between river-induced flushing and
320 upstream transport of marine SPM, as a function of estuarine geomorphology, gravitational circulation and tidal
321 flow, trapping the particles in the MTZ (Bianchi, 2007; Sommerfield and Wong, 2011; Winterwerp and Wang,
322 2013). Other studies detected N_2O production from water column nitrification in estuarine MTZs (e.g. Barnes and
323 Owens, 1999; de Wilde and de Bie, 2000; Bange, 2006; Barnes and Upstill-Goddard, 2011; Harley et al., 2015),
324 caused by high bacterial numbers, particulate nitrogen availability and long residence times (Murray et al., 2015).
325 For the selected dataset, we calculated a negative correlation between average SPM concentrations and N_2O
326 saturation ($R = -0.81$, Table 5), and found that the N_2O peak was located downstream of the MTZ, and upstream
327 of increasing nitrite and ammonium concentrations (Fig. 4a). This suggests that (1) the mere concentration of SPM
328 is not the driving factor of nitrification as a source of N_2O , but that organic matter quality is key to biological
329 turnover (Dähnke et al. 2022), and (2) the material transport from the North Sea upstream towards the MTZ
330 (Kappenberg and Fanger, 2007; Schoer, 1990) is a main mechanism for N_2O generation. We find organic matter
331 with low C/N ratios, and with relatively high PN and PC contents in the outermost samples (ranging from 5.9 in
332 June 2020 to 8.8 August 2017), indicating fresh and easily degradable organic matter (Fig. S1, e.g. Redfield et al.
333 1963; Fraga et al. 1998; Middelburg and Herman 2007). Towards the MTZ, C/N values, PN and PC contents
334 decreased, indicating remineralization in the water column. This remineralization and subsequent nitrification can
335 then cause the observed succession of ammonium, nitrite and N_2O peaks (Fig. 4a), contributing to the high nitrate
336 concentrations in the MTZ, where high C/N values (9 – 11/16) indicate low organic matter quality (e.g. Hedges
337 and Keil 1995; Middelburg and Herman 2007). Overall, we conclude that remineralization of marine organic
338 matter, followed by nitrification, produced the N_2O peak in the salinity gradient of the Elbe Estuary. This
339 production was mainly fueled by fresh organic matter entering the estuary from the North Sea.

340 **4.3 Hamburg Port: N_2O production in spring and summer**

341 During all cruises, we measured highest N_2O saturation in the Port of Hamburg. These peaks can be caused by
342 input from a waste water treatment plant, by deepening and dredging operations, enhanced benthic production or
343 by in-situ production in the water column.

344 Point sources generally play a minor role in the Elbe Estuary (Hofmann et al., 2005; IKSE, 2018). We estimated
345 the wastewater discharge fraction of stream flow according to Büttner et al. (2020) for the waste water treatment
346 plant (WWTP) Köhlbrandhöft, which treats the waste water from the Hamburg metropolitan region, with less than
347 5 % even under low fresh water inflow. Thus, point sources seemed not to be the cause for the elevated N_2O
348 concentrations. [However, discharge of WWTPs can potentially be important sources of \$\text{N}_2\text{O}\$](#) (Beaulieu et al., 2010;
349 Chun et al., 2020; Brown et al., 2022), [and the effect of wastewater input on \$\text{N}_2\text{O}\$ concentrations and emissions](#)
350 [may change with altered river discharge, water temperature and riverine nitrogen loads in the future.](#)

351 Dredging can be a potential source of N_2O in the water column. The estuary is continuously deepened and dredged
352 to grant access for large container ships, which stirs up bottom sediments. Ammonium concentrations in the

353 sediment pore water are high (Zander et al., 2020, 2022) and N₂O can be produced by nitrifier-denitrification in
354 the sediments (Deek et al., 2013). However, we found no correlation of high SPM concentrations and N₂O
355 saturation, indicating no major influence on N₂O dynamics from channel dredging and deepening.

356 Several studies identified the Hamburg Port region as a hotspot of biogeochemical turnover: Deek et al. (2013)
357 showed denitrification, where Sanders et al. (2018) measured intense nitrification.. Norbistrath et al. (2022)
358 determined intense total alkalinity generation, and Dähnke et al. (2022) found that nitrogen turnover was driven
359 by high particulate organic matter in this region. Brase et al. (2017) identified the Hamburg port region as a hotspot
360 of N₂O production and hypothesized that simultaneous nitrification and sediment denitrification were responsible.
361 We use our expanded dataset to further evaluate this hypothesis and to identify drivers for N₂O production in the
362 port region.

363 During all cruises in spring and summer, we measured ammonium and nitrite peaks in the Hamburg Port region
364 (Fig. 2c and 2e, exemplary for September 2020 in Fig. 4b). Several researchers did address the nitrogen turnover
365 and this accumulation of nitrite and ammonium assuming that the sudden increase of water depth in the Port leads
366 to a light limitation and decomposition of riverine organic material (Schroeder, 1997; Schöl et al., 2014). This in
367 turn raises ammonium and nitrite concentrations and fosters nitrification in the port region (Sanders et al., 2018;
368 Dähnke et al., 2022).

369 High nitrite concentrations are favorable for N₂O production by ~~nitrification and~~ nitrifier-denitrification (Quick et
370 al., 2019), while low-oxygen conditions facilitate N₂O production from both nitrification and denitrification. We
371 found that N₂O saturation increased with decreasing discharge (R = -0.48, Table 5) during spring and summer.
372 This further points towards in-situ N₂O production, because ~~denitrification and nitrification are more intense during~~
373 longer residence times lead to a possible accumulation of N₂O from either nitrification or denitrification (e.g.
374 Nixon et al. 1996; Pind et al. 1997; Silvennoinen et al. 2007; Gonçalves et al. 2010). Overall, our data showed the
375 succession of ammonium, nitrite and N₂O production (Fig. 4b and supplementary material ~~S3S4-S13S14~~) as well
376 as a breakup of the linear relation between AOU and N₂O_{xs} in the Port region (Fig. 3). In combination with previous
377 nitrogen process studies performed in the Elbe Estuary (Deek et al., 2013; Sanders et al., 2018; Dähnke et al.,
378 2022), this supports simultaneous sedimentary denitrification and nitrification in the water column as responsible
379 pathways for N₂O production in the Port of Hamburg (Brase et al. 2017).

380 In spring and summer, we found no linear relationship between N₂O_{xs} and AOU in the Hamburg Port (Fig. 3). This
381 may result from combined N₂O production by nitrification and denitrification. However, oxygen saturation and
382 N₂O saturation were inversely correlated in Hamburg Port (Table 4 and 5), suggesting that N₂O production was
383 controlled by oxygen concentrations, and thus was related to oxygen consumption in the port region. Most (75 %)
384 of this oxygen consumption is caused by respiration whereas the remaining 25 % stem from nitrification (Schöl et
385 al., 2014; Sanders et al., 2018). This respiration in turn is determined by remineralization of algal material from
386 the upstream river that is transported to and respired within the port region (Schroeder, 1997; Kerner, 2000; Schöl
387 et al., 2014), linking estuarine N₂O production to river eutrophication. Fabisik et al. (2023) showed that algae could
388 additionally contribute to N₂O production. In the Elbe, fresh organic matter from the river with low C/N values as
389 well as high PN and PC contents entered the estuary. This organic material was rapidly degraded in the Hamburg
390 Port region (Fig. S1). Dähnke et al. (2022) found that labile organic matter fueled nitrification but also
391 denitrification in the fresh water part of the Elbe Estuary, which, as shown in our study, results in high N₂O
392 production in the Hamburg Port, leading to the reported negative correlations of PC and PN content with N₂O
393 saturation.

394 Overall, oxygen conditions mainly controlled N₂O production in the Hamburg Port region in spring and summer.
395 Since respiration of organic matter dominates oxygen drawdown in the port region, we deduce that N₂O production
396 there is linked to the decomposition of phytoplankton produced in the upstream Elbe River regions.

397 **4.4 Hamburg Port: N₂O production in winter**

398 In winter, low water temperature (< 6 °C) should hamper biological production (Koch et al., 1992; Halling-
399 Sorensen and Jorgensen, 1993). Indeed, we did not detect a N₂O peak in the MTZ in winter, but we find high N₂O
400 concentrations in the port region. For March 2022, we found a linear increase of N₂O_{xs} and AOU along with
401 oxygen consumption and increasing ammonium, nitrite and PN concentrations indicating nitrification in the
402 Hamburg Port producing N₂O. Unlike in summer, N₂O concentrations showed a flat increase extending far into
403 the oligohaline section of the estuary (Fig. 2, -Fig. S1).

404 However, in March 2021, we found a sharp and sudden increase in N₂O, with a peak concentration that by far
405 exceeded internal biological sources in summer (Fig. 2h). An ammonium peak in the water column coincided with
406 the N₂O maximum (Fig. 2f and Fig. [S4+S12](#)). If microbial activity is mostly temperature-inhibited, a local source
407 of N₂O in the port seems the most likely cause.

408 We considered intensified deepening operations in the Port of Hamburg [as](#) one potential source of elevated N₂O
409 saturation. Deepening and dredging work occurred in the Hamburg Port region in 2021 (HPA, pers. Comm.,
410 Karrasch 2022), but, this also applied to 2022, when we saw no sharp N₂O peak (Fig. 2h). Furthermore, the regions
411 of deepening and dredging did not match the region of high N₂O concentrations, and turbidity at the time of
412 sampling did not change significantly compared to other cruises. Jointly, this suggests that channel dredging and
413 deepening was not the primary cause for the 2021 winter N₂O peak.

414 Another possible source of N₂O is the WWTP outflow in the Southern Elbe that joins the -main estuary at stream
415 kilometer 626 (Fig. 1), matching the N₂O peak at stream kilometer 627 (Fig. 2h). As explained above (section 4.3),
416 the effect of this WWTP on N₂O saturations under normal conditions should be negligible. This peak can be the
417 result of an extraordinary event during our sampling. We indeed found that an extreme rain event occurred on
418 March 11th 2021 (HAMBURG WASSER, pers. Comm., Laurich 2022) with a statistical recurrence probability of
419 one to five years (<https://sri.hamburgwasser.de/>, last access: 04.04.2023). This rare event caused [a temperature](#)
420 [drop in the WWTP due to high inflows of cold rainwater leading to](#) aggravated operation conditions [in the WWTP](#)
421 at the time of sampling. While the operators could still meet the limits for the effluent levels of nitrate and
422 ammonium, higher than usual ammonium loads exited the treatment plant at this time. We [assume-hypothesize](#)
423 that these elevated ammonium WWTP loads, were rapidly converted to N₂O as the warmer and biologically active
424 waste water entered the Elbe Estuary in March 2021. [An important factor for aggravated conditions was a](#)
425 [temperature drop in the WWTP caused by cold rain water \(HAMBURG WASSER, pers. Comm., Laurich 2022\),](#)
426 [we therefore](#) hypothesize that a similar rain event in warmer months would not [lead to comparable N₂O peaks](#)
427 [have the same effect.](#)

428 Therefore, we argue that our March 2021 cruise likely represents an exception due to an extreme weather situation,
429 whereas normal winter conditions in the estuary comply with the N₂O production, like in March 2022.

430 **4.5 Seasonally varying N₂O:DIN dynamic**

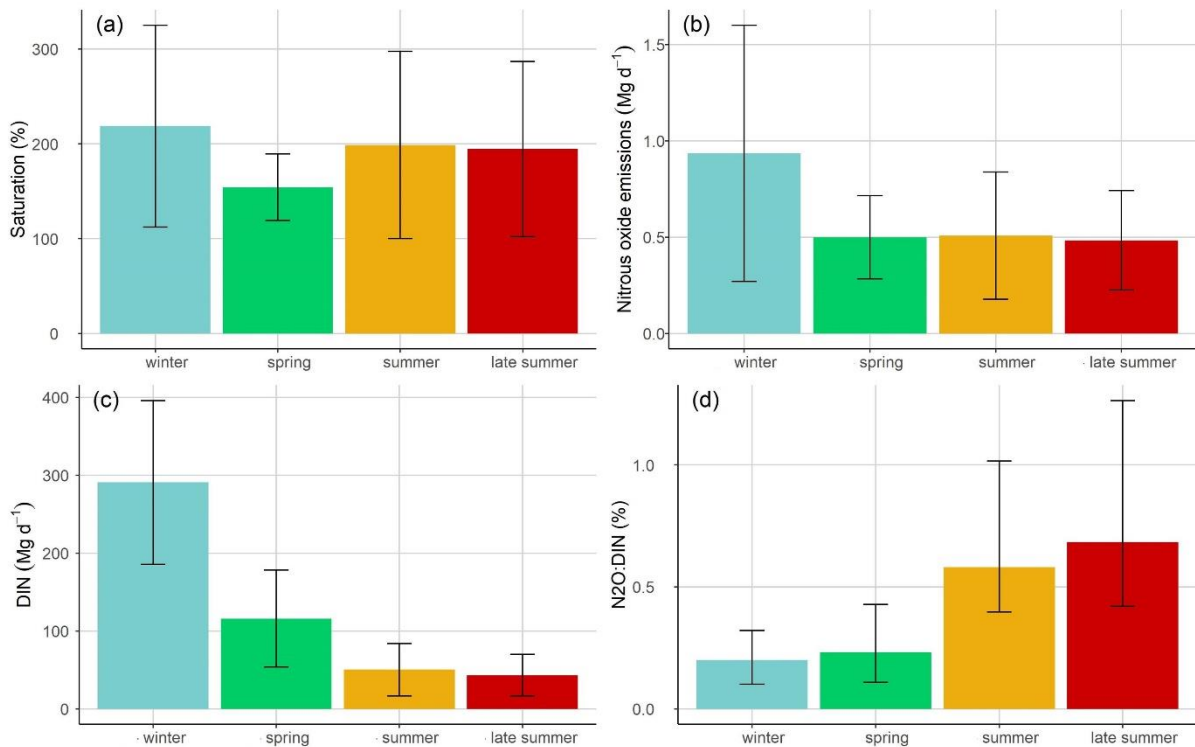
431 We calculated annual N₂O emissions of the Elbe Estuary ranging from 0.08 ± 0.03 Gg-N₂O yr⁻¹ to
432 0.25 ± 0.16 Gg-N₂O yr⁻¹, which varied from recent N₂O summer emission estimate of 0.18 ± 0.01 Gg-N₂O yr⁻¹ by

433 Brase et al. (2017). Estuarine N₂O emissions are affected by tides, diel variations and currents (Barnes et al., 2006;
434 Baulch et al., 2012; Gonçalves et al., 2015), all of which we did not address in our study. Range of possible
435 parametrizations of gas transfer coefficients further complicates a direct comparison of fluxes between studies
436 (Hall Jr. and Ulseth, 2020; Rosentreter et al., 2021), which ~~were~~ was reflected in the big differences of our emission
437 estimates (Table 2). Therefore, a direct comparison to other studies is difficult.

438 In a more general approach, the relationship between N₂O and DIN (N₂O:DIN) is used for global estimates of N₂O
439 emissions (Kroeze et al., 2005, 2010; Ivens et al., 2011; Hu et al., 2016). Using publicly available data (Table S4
440 and S5), we calculated the amount of the annual nitrogen load released as N₂O. Depending on the parametrization
441 used for the gas transfer coefficients, 0.14 % to 0.67 % of the annual DIN loads of the Elbe Estuary were released
442 as N₂O (0.11 % to 0.57 % for TN loads). This is significantly less than the 1 % predicted by Kroeze et al. (2005),
443 but matches results from other estuaries with high agricultural input, e.g. Wells et al. (2018) with 0.3 % to 0.7 %
444 (0.1 % for TN loads) and Robinson et al. (1998) with 0.5 % (0.3 % for TN loads) as well as the 0.11 % to 0.37 %
445 estimated by Maavara et al. (2019), who used TN loads to predict global estuarine emissions. In general, N₂O:DIN
446 ratios vary widely (e.g., Baulch et al., 2012; Maavara et al., 2019; Smith and Böhlke, 2019). ~~(Wells et al., (2018)~~
447 even found a range from -25 % to 7 % of DIN was emitted as N₂O in estuaries with low land-use intensity.

448 At our site, highest emissions were estimated in winter (Fig. 5b) along with highest DIN loads (Fig. 5c). In spring,
449 summer and late summer, N₂O emissions reduced along with DIN loads (Fig. 5b, c). However, N₂O release did
450 not scale with the seasonal change of DIN. In winter, 0.10 % to 0.32 % of DIN were released as N₂O, whereas
451 during the other seasons, up to 1.26 % were emitted. Thus, our results corroborate that there is a deviating-varying
452 relationship between DIN and N₂O (Borges et al., 2015; Marzadri et al., 2017; Wells et al., 2018) showing that
453 this relationship even varies seasonally on site due to changing drivers for N₂O production and emissions, e.g.,
454 temperature (Murray et al., 2015; Quick et al., 2019) and oxygen levels (de Bie et al., 2002; Rosamond et al., 2012;
455 Yevenes et al., 2017).

456 Next to DIN loads, we find that organic matter is an important driver for N₂O production by providing substrate
457 for nitrification. Furthermore, the comparison of ~~our~~ results with previous measurements in the Elbe Estuary
458 revealed that N₂O saturation stopped to scale with DIN input after the 1990s (section 4.1). The significant regime
459 change after the 1990s enabled phytoplankton growth to reestablish in the river that had previously been inhibited
460 by high pollutant levels and low light availability (Kerner, 2000; Amann et al., 2012; Hillebrand et al., 2018;
461 Rewrie et al., submitted). ~~and led to h~~ The prevailing high nitrification rates in the estuary (Dähnke et al., 2008;
462 Sanders et al., 2018) support, supporting the an overarching control of organic matter on N₂O production and
463 emissions along the Elbe Estuary.



464
 465 **Figure 5: (a) Average nitrous oxide saturation for each season, (b) average nitrous oxide emissions for each season**
 466 **calculated after Borges et al. (2004), (c) average DIN loads for each season and (d) ratio of nitrous oxide emissions and**
 467 **DIN loads (N₂O:DIN) for each season. The error bars represent the standard deviations for (a), (b) and (c). The**
 468 **N₂O:DIN ratios is shown as average values calculated for each parametrization and wind speeds with error bars**
 469 **representing their variability.**

470 **5 Conclusions**

471 Overall, the Elbe is a year-round source of N₂O to the atmosphere, with highest emissions occurring in winter,
 472 along with high DIN loads and high wind speeds. However, summer N₂O saturation and emissions did not decrease
 473 with lower riverine nitrogen input, suggesting variable relations of DIN and N₂O (Borges et al., 2004; Marzadri et
 474 al., 2017; Wells et al., 2018), and seasonal variability of this ratio caused by changing drivers for N₂O production
 475 and emissions. Two hot-spots of N₂O production were found in the Elbe Estuary: the Port of Hamburg and the
 476 mesohaline estuary near the estuarine turbidity maximum. Biological N₂O production was enhanced by warmer
 477 temperatures and fueled by riverine organic matter in the Hamburg Port or marine organic matter in the MTZ. A
 478 comparison with historical N₂O measurements in the Elbe Estuary revealed that N₂O saturation did not decrease
 479 with DIN input after the 1990s. The improvement of water quality in the Elbe Estuary allowed phytoplankton
 480 growth after the reunification of Germany in 1990s (Kerner, 2000; Amann et al., 2012; Hillebrand et al., 2018;
 481 Rewrie et al., submitted) and led to a switch from dominant denitrification to high nitrification (Dähnke et al.,
 482 2008; Sanders et al., 2018), supporting the overarching control of organic matter on N₂O production along the
 483 Elbe Estuary. Thus, our findings indicate that DIN availability is not the sole control of N₂O production in estuaries
 484 with high agricultural input.

485 High organic matter availability due to phytoplankton blooms driven by river eutrophication fuels nitrification and
 486 subsequent N₂O emissions, causing a decoupling of the N₂O:DIN ratio. Therefore, N₂O emissions in heavily
 487 managed estuaries with high agricultural loads are clearly linked to eutrophication. A reduced nitrogen input would
 488 reduce phytoplankton growth and thus also N₂O emissions. However, the development of phytoplankton blooms
 489 is not solely controlled by nutrient inputs, but also by e.g., temperature, residence time, water depth and grazing.

490 [Thus, complex biological and chemical processes control phytoplankton dynamics \(Scharfe et al., 2009; Dijkstra](#)
491 [et al., 2019; Kamjunke et al., 2021\), which will change significantly in the future due to the effects of climate](#)
492 [change \(IPCC, 2022\). A holistic approach to water quality mitigation and climate change adaptation is needed to](#)
493 [prevent high N₂O emissions. High organic matter availability due to phytoplankton blooms driven by river](#)
494 [eutrophication fuels nitrification and subsequent N₂O emissions, causing a decoupling of the N₂O:DIN ratio.](#)
495 [Therefore, N₂O emissions in heavily managed estuaries with high agricultural loads are clearly linked to](#)
496 [eutrophication. Consequently, reducing nitrogen input alone is not sufficient to minimize N₂O emissions from](#)
497 [estuaries. Further measures are needed to prevent the developments of intense phytoplankton blooms in rivers and](#)
498 [estuaries. Especially considering climate change projections of more frequent and extensive draughts and warmer](#)
499 [temperatures \(IPCC, 2022\), which potentially fuel phytoplankton growth.](#)

500

501 **Data availability**

502 The dataset generated and/or analyzed in this study are currently available upon request from the corresponding
503 author and will be made publicly available under coastMap Geoportal (www.coastmap.org) connecting to
504 PANGAEA. (<https://www.pangaea.de/>) with DOI availability in the near future.

505 **Authors contribution**

506 GS, TS and KD designed this study. GS did the sampling and measurements for cruises from 2020 to 2022 as well
507 as the data interpretation and evaluation. TS was responsible for the sampling and measurements for cruises done
508 in 2017 and 2019. YGV provided the oxygen data correction from the FerryBox data. KD, HWB, YGV and TS
509 contributed with scientific and editorial recommendations. GS prepared the manuscript with contributions of all
510 co-authors.

511 **Competing interest**

512 The authors declare that they have no conflict of interest.

513 **Acknowledgments**

514 This study was funded by the Deutsche Forschungsgemeinschaft (DFG, German Research Foundation) under
515 Germany's Excellence Strategy – EXC 2037 “CLICCS - Climate, Climatic Change, and Society” – Project
516 Number: 390683824, contribution to the Center for Earth System Research and Sustainability (CEN) of Universität
517 Hamburg. Parts of the study were done in the framework of the cross-topic activity MOSES (Modular Observation
518 Solutions for Earth Systems) within the Helmholtz program Changing Earth (Topic 4.1). We thank the crew of
519 R/V Ludwig Prandtl for the great support during the cruises. Thanks to Leon Schmidt and the entire working group
520 “Aquatic nutrients cycles” for measuring nutrients and the support during the campaigns. We are thankful for the
521 Hereon FerryBox Team for providing the FerryBox data. Thanks to the working group of Biogeochemistry at the
522 Institute for Geology of the University Hamburg for measuring C/N ratios, PC and PN fractions. We thank Frank
523 Laurich (HAMBURG WASSER) and Dr. Maja Karrasch (Hamburg Port Authority) for their interest in our N₂O

524 measurements and their willingness to provide information. Thanks to Victoria Oritz (Federal Waterways and
525 Engineering and Research Institute) for providing the respective areas of the Elbe Estuary. Thanks to the NOAA
526 ESRL GML CCGG Group for providing high quality, readily accessible atmospheric N₂O data.

527 **References**

- 528 Amann, T., Weiss, A., and Hartmann, J.: Carbon dynamics in the freshwater part of the Elbe estuary, Germany:
529 Implications of improving water quality, *Estuar. Coast. Shelf Sci.*, 107, 112–121,
530 <https://doi.org/10.1016/j.ecss.2012.05.012>, 2012.
- 531 Bange, H. W.: Nitrous oxide and methane in European coastal waters, *Estuar. Coast. Shelf Sci.*, 70, 361–374,
532 <https://doi.org/10.1016/j.ecss.2006.05.042>, 2006.
- 533 Bange, H. W.: Chapter 2 - Gaseous Nitrogen Compounds (NO, N₂O, N₂, NH₃) in the Ocean, *Nitrogen Mar.*
534 *Environ. Second Ed.*, 51–94, <https://doi.org/10.1016/B978-0-12-372522-6.00002-5>, 2008.
- 535 Barnes, J. and Owens, N. J. P.: Denitrification and Nitrous Oxide Concentrations in the Humber Estuary, UK, and
536 Adjacent Coastal Zones, *Mar. Pollut. Bull.*, 37, 247–260, [https://doi.org/10.1016/S0025-326X\(99\)00079-X](https://doi.org/10.1016/S0025-326X(99)00079-X), 1999.
- 537 Barnes, J. and Upstill-Goddard, R. C.: N₂O seasonal distributions and air-sea exchange in UK estuaries:
538 Implications for the tropospheric N₂O source from European coastal waters, *J. Geophys. Res. Biogeosciences*,
539 116, <https://doi.org/10.1029/2009JG001156>, 2011.
- 540 Barnes, J., Ramesh, R., Purvaja, R., Nirmal Rajkumar, A., Senthil Kumar, B., Krithika, K., Ravichandran, K.,
541 Uher, G., and Upstill-Goddard, R.: Tidal dynamics and rainfall control N₂O and CH₄ emissions from a pristine
542 mangrove creek, *Geophys. Res. Lett.*, 33, <https://doi.org/10.1029/2006GL026829>, 2006.
- 543 Baulch, H. M., Dillon, P. J., Maranger, R., Venkiteswaran, J. J., Wilson, H. F., and Schiff, S. L.: Night and day:
544 short-term variation in nitrogen chemistry and nitrous oxide emissions from streams, *Freshw. Biol.*, 57, 509–525,
545 <https://doi.org/10.1111/j.1365-2427.2011.02720.x>, 2012.
- 546 BAW Oritz, V.: pers. Comm.: Flächen des Elbe Ästuars, 2023.
- 547 Beaulieu, J. J., Shuster, W. D., and Rebolz, J. A.: Nitrous Oxide Emissions from a Large, Impounded River: The
548 Ohio River, *Environ. Sci. Technol.*, 44, 7527–7533, <https://doi.org/10.1021/es1016735>, 2010.
- 549 Bergemann, M.: Die Trübungszone in der Tideelbe - Beschreibung der räumlichen und zeitlichen Entwicklung,
550 Wassergütestelle Elbe, 2004.
- 551 Bergemann, M. and Gaumert, T.: Elbebericht 2008: Ergebnisse des nationalen Überwachungsprogramms Elbe der
552 Bundesländer über den ökologischen und chemischen Zustand der Elbe nach EG-WRRL sowie der
553 Trendentwicklung von Stoffen und Schadstoffgruppen, Flussgebietsgemeinschaft Elbe (FGG Elbe), Hamburg,
554 2008.
- 555 van Beusekom, J. E. E., Carstensen, J., Dolch, T., Grage, A., Hofmeister, R., Lenhart, H., Kerimoglu, O., Kolbe,
556 K., Pätsch, J., Rick, J., Rönn, L., and Ruiter, H.: Wadden Sea Eutrophication: Long-Term Trends and Regional
557 Differences, *Front. Mar. Sci.*, 6, 370, <https://doi.org/10.3389/fmars.2019.00370>, 2019.
- 558 Bianchi, T. S.: *Biogeochemistry of Estuaries*, Oxford University Press, New York, 706 pp.,
559 <https://doi.org/10.1093/oso/9780195160826.001.0001>, 2007.
- 560 de Bie, M. J. M., Middelburg, J. J., Starink, M., and Laanbroek, H. J.: Factors controlling nitrous oxide at the
561 microbial community and estuarine scale, *Mar. Ecol. Prog. Ser.*, 240, 1–9, <https://doi.org/10.3354/meps240001>,
562 2002.
- 563 Boehlich, M. J. and Strotmann, T.: The Elbe Estuary, *Küste*, 74, 288–306, 2008.

- 564 Boehlich, M. J. and Strotmann, T.: Das Elbeästuar, Küste, 87, Kuratorium für Forschung im Küsteningenieurwesen
565 (KFKI), <https://doi.org/10.18171/1.087106>, 2019.
- 566 Borges, A., Vanderborght, J.-P., Schiettecatte, L.-S., Gazeau, F., Ferrón-Smith, S., Delille, B., and Frankignoulle,
567 M.: Variability of gas transfer velocity of CO₂ in a macrotidal estuary (The Scheldt), *Estuaries*, 27, 593–603,
568 <https://doi.org/10.1007/BF02907647>, 2004.
- 569 Borges, A. V., Darchambeau, F., Teodoru, C. R., Marwick, T. R., Tamooh, F., Geeraert, N., Omengo, F. O.,
570 Guérin, F., Lambert, T., Morana, C., Okuku, E., and Bouillon, S.: Globally significant greenhouse-gas emissions
571 from African inland waters, *Nat. Geosci.*, 8, 637–642, <https://doi.org/10.1038/ngeo2486>, 2015.
- 572 Bouwman, A. F., Bierkens, M. F. P., Griffioen, J., Hefting, M. M., Middelburg, J. J., Middelkoop, H., and Slomp,
573 C. P.: Nutrient dynamics, transfer and retention along the aquatic continuum from land to ocean: towards
574 integration of ecological and biogeochemical models, *Biogeosciences*, 10, 1–23, [https://doi.org/10.5194/bg-10-1-](https://doi.org/10.5194/bg-10-1-2013)
575 2013, 2013.
- 576 Brase, L., Bange, H. W., Lendt, R., Sanders, T., and Dähnke, K.: High Resolution Measurements of Nitrous Oxide
577 (N₂O) in the Elbe Estuary, *Front. Mar. Sci.*, 4, 162, <https://doi.org/10.3389/fmars.2017.00162>, 2017.
- 578 Brown, A. M., Bass, A. M., and Pickard, A. E.: Anthropogenic-estuarine interactions cause disproportionate
579 greenhouse gas production: A review of the evidence base, *Mar. Pollut. Bull.*, 174, 113240,
580 <https://doi.org/10.1016/j.marpolbul.2021.113240>, 2022.
- 581 Büttner, O., Jawitz, J. W., and Borchardt, D.: Ecological status of river networks: stream order-dependent impacts
582 of agricultural and urban pressures across ecoregions, *Environ. Res. Lett.*, 15, 1040b3,
583 <https://doi.org/10.1088/1748-9326/abb62e>, 2020.
- 584 Chun, Y., Kim, D., Hattori, S., Toyoda, S., Yoshida, N., Huh, J., Lim, J.-H., and Park, J.-H.: Temperature control
585 on wastewater and downstream nitrous oxide emissions in an urbanized river system, *Water Res.*, 187, 116417,
586 <https://doi.org/10.1016/j.watres.2020.116417>, 2020.
- 587 Clark, J. F., Schlosser, P., Simpson, H. J., Stute, M., Wanninkhof, R., and Ho, D. T.: Relationship between gas
588 transfer velocities and wind speeds in the tidal Hudson River determined by the dual tracer technique, in: *Air-*
589 *Water Gas Transfer*, edited by: Jähne, B. and Monahan, E. C., AEON Verlag, Hanau, 785–800, 1995.
- 590 Crossland, C. J., Baird, D., Ducrotoy, J.-P., Lindeboom, H., Buddemeier, R. W., Dennison, W. C., Maxwell, B.
591 A., Smith, S. V., and Swaney, D. P.: The Coastal Zone — a Domain of Global Interactions, in: *Coastal Fluxes in*
592 *the Anthropocene: The Land-Ocean Interactions in the Coastal Zone Project of the International Geosphere-*
593 *Biosphere Programme*, edited by: Crossland, C. J., Kremer, H. H., Lindeboom, H. J., Marshall Crossland, J. I., and
594 Tissier, M. D. A., Springer, Berlin, Heidelberg, 1–37, https://doi.org/10.1007/3-540-27851-6_1, 2005.
- 595 Dähnke, K., Bahlmann, E., and Emeis, K.-C.: A nitrate sink in estuaries? An assessment by means of stable nitrate
596 isotopes in the Elbe estuary, *Limnol. Oceanogr.*, 53, 1504–1511, <https://doi.org/10.4319/lo.2008.53.4.1504>, 2008.
- 597 Dähnke, K., Sanders, T., Voynova, Y., and Wankel, S. D.: Nitrogen isotopes reveal a particulate-matter-driven
598 biogeochemical reactor in a temperate estuary, *Biogeosciences*, 19, 5879–5891, [https://doi.org/10.5194/bg-19-](https://doi.org/10.5194/bg-19-5879-2022)
599 5879-2022, 2022.
- 600 Deek, A., Dähnke, K., van Beusekom, J., Meyer, S., Voss, M., and Emeis, K.-C.: N₂ fluxes in sediments of the
601 Elbe Estuary and adjacent coastal zones, *Mar. Ecol. Prog. Ser.*, 493, 9–21, <https://doi.org/10.3354/meps10514>,
602 2013.
- 603 Dijkstra, Y. M., Chant, R. J., and Reinfelder, J. R.: Factors Controlling Seasonal Phytoplankton Dynamics in the
604 Delaware River Estuary: an Idealized Model Study, *Estuaries Coasts*, 42, 1839–1857,
605 <https://doi.org/10.1007/s12237-019-00612-3>, 2019.
- 606 Dlugokencky, E. J., Crotwell, A. M., Mund, J. W., Crotwell, M. J., and Thoning, K. W.: Earth System Research
607 Laboratory Carbon Cycle and Greenhouse Gases Group Flask-Air Sample Measurements of N₂O at Global and
608 Regional Background Sites, 1967-Present [Data set], <https://doi.org/10.15138/53G1-X417>, 2022.

- 609 Fabisik, F., Guieysse, B., Procter, J., and Plouviez, M.: Nitrous oxide (N₂O) synthesis by the freshwater
610 cyanobacterium *Microcystis aeruginosa*, *Biogeosciences*, 20, 687–693, <https://doi.org/10.5194/bg-20-687-2023>,
611 2023.
- 612 FGG Elbe: Nährstoffminderungsstrategie für die Flussgebietsgemeinschaft Elbe, Flussgebietsgemeinschaft Elbe
613 (FGG Elbe), Magdeburg, 2018.
- 614 Das Fachinformationssystem (FIS) der FGG Elbe: [https://www.elbe-
615 datenportal.de/FisFggElbe/content/start/ZurStartseite.action;jsessionid=A37EDCF5B5EC1ECB15091447E64EC
616 538](https://www.elbe-

615 datenportal.de/FisFggElbe/content/start/ZurStartseite.action;jsessionid=A37EDCF5B5EC1ECB15091447E64EC

616 538), last access: 21 November 2022.
- 617 Fraga, F., Ríos, A. F., Pérez, F. F., and Figueiras, F. G.: Theoretical limits of oxygen:carbon and oxygen:nitrogen
618 ratios during photosynthesis and mineralisation of organic matter in the sea, *Sci. Mar.*, 62, 161–168,
619 <https://doi.org/10.3989/scimar.1998.62n1-2161>, 1998.
- 620 Garnier, J., Cébron, A., Tallec, G., Billen, G., Sebilo, M., and Martinez, A.: Nitrogen Behaviour and Nitrous Oxide
621 Emission in the Tidal Seine River Estuary (France) as Influenced by Human Activities in the Upstream Watershed,
622 *Biogeochemistry*, 77, 305–326, <https://doi.org/10.1007/s10533-005-0544-4>, 2006.
- 623 Gaumert, T. and Bergemann, M.: Sauerstoffgehalt der Tideelbe - Entwicklung der kritischen Sauerstoffgehalte im
624 Jahr 2007 und in den Vorjahren, Erörterung möglicher Ursachen und Handlungsoptionen,
625 Flussgebietsgemeinschaft Elbe, 2007.
- 626 Geerts, L., Wolfstein, K., Jacobs, S., van Damme, S., and Vandenbruwaene, W.: Zonation of the TIDE estuaries,
627 TIDE toolbox, 2012.
- 628 Gonçalves, C., Brogueira, M. J., and Camões, M. F.: Seasonal and tidal influence on the variability of nitrous oxide
629 in the Tagus estuary, Portugal, *Sci. Mar.*, 74, 57–66, <https://doi.org/10.3989/scimar.2010.74s1057>, 2010.
- 630 Gonçalves, C., Brogueira, M. J., and Nogueira, M.: Tidal and spatial variability of nitrous oxide (N₂O) in Sado
631 estuary (Portugal), *Estuar. Coast. Shelf Sci.*, 167, 466–474, <https://doi.org/10.1016/j.ecss.2015.10.028>, 2015.
- 632 Hall Jr., R. O. and Ulseth, A. J.: Gas exchange in streams and rivers, *WIREs Water*, 7, e1391,
633 <https://doi.org/10.1002/wat2.1391>, 2020.
- 634 Halling-Sorensen, B. and Jorgensen, S. E. (Eds.): 3. Process Chemistry and Biochemistry of Nitrification, in:
635 *Studies in Environmental Science*, vol. 54, Elsevier, 55–118, [https://doi.org/10.1016/S0166-1116\(08\)70525-9](https://doi.org/10.1016/S0166-1116(08)70525-9),
636 1993.
- 637 HAMBURG WASSER, Laurich, F.: pers. Comm.: N₂O in der Elbe, 2022.
- 638 Hanke, V.-R. and Knauth, H.-D.: N₂O-Gehalte in Wasser-und Luftproben aus den Bereichen der Tideelbe und der
639 Deutschen Bucht, GKSS-Forschungszentrum, Weinheim, 1990.
- 640 Hansen, H. P. and Koroleff, F.: Determination of nutrients, in: *Methods of Seawater Analysis*, John Wiley & Sons,
641 Ltd, 159–228, <https://doi.org/10.1002/9783527613984.ch10>, 1999.
- 642 Harley, J. F., Carvalho, L., Dudley, B., Heal, K. V., Rees, R. M., and Skiba, U.: Spatial and seasonal fluxes of the
643 greenhouse gases N₂O, CO₂ and CH₄ in a UK macrotidal estuary, *Estuar. Coast. Shelf Sci.*, 153, 62–73,
644 <https://doi.org/10.1016/j.ecss.2014.12.004>, 2015.
- 645 Hedges, J. I. and Keil, R. G.: Sedimentary organic matter preservation: an assessment and speculative synthesis,
646 *Mar. Chem.*, 49, 81–115, [https://doi.org/10.1016/0304-4203\(95\)00008-F](https://doi.org/10.1016/0304-4203(95)00008-F), 1995.
- 647 Hein, S. S. V., Sohr, V., Nehlsen, E., Strotmann, T., and Fröhle, P.: Tidal Oscillation and Resonance in Semi-
648 Closed Estuaries—Empirical Analyses from the Elbe Estuary, North Sea, *Water*, 13, 848,
649 <https://doi.org/10.3390/w13060848>, 2021.
- 650 Schleswig-Holstein u. Hamburg: Mittlere Windgeschwindigkeit (1986-2015)* | Norddeutscher Klimamonitor:
651 [https://www.norddeutscher-klimamonitor.de/klima/1986-2015/jahr/mittlere-windgeschwindigkeit/schleswig-
652 holstein-hamburg/coastdat-1.html](https://www.norddeutscher-klimamonitor.de/klima/1986-2015/jahr/mittlere-windgeschwindigkeit/schleswig-

652 holstein-hamburg/coastdat-1.html), last access: 27 April 2023.

653 Hillebrand, G., Hardenbicker, P., Fischer, H., Otto, W., and Vollmer, S.: Dynamics of total suspended matter and
654 phytoplankton loads in the river Elbe, *J. Soils Sediments*, 18, 3104–3113, [https://doi.org/10.1007/s11368-018-](https://doi.org/10.1007/s11368-018-1943-1)
655 1943-1, 2018.

656 Hofmann, J., Behrendt, H., Gilbert, A., Janssen, R., Kannen, A., Kappenberg, J., Lenhart, H., Lise, W., Nunneri,
657 C., and Windhorst, W.: Catchment–coastal zone interaction based upon scenario and model analysis: Elbe and the
658 German Bight case study, *Reg. Environ. Change*, 5, 54–81, <https://doi.org/10.1007/s10113-004-0082-y>, 2005.

659 HPA and Freie und Hansestadt Hamburg: Deutsches Gewässerkundliches Jahrbuch - Elbegebiet, Teil III, Untere
660 Elbe ab der Havelmündung - 2014, Hamburg, 2017.

661 HPA, Karrasch, M.: pers. Comm.: Anfrage wegen N₂O Peak - Baggararbeiten Elbe März 2021 und März 2022,
662 2022.

663 Hu, M., Chen, D., and Dahlgren, R. A.: Modeling nitrous oxide emission from rivers: a global assessment, *Glob.*
664 *Change Biol.*, 22, 3566–3582, <https://doi.org/10.1111/gcb.13351>, 2016.

665 IKSE: Strategie zur Minderung der Nährstoffeinträge in Gewässer in der internationalen Flussgebietsgemeinschaft
666 Elbe, Internationale Kommission zur Schutz der Elbe, Magdeburg, 2018.

667 IPCC: Climate Change 2021: The Physical Science Basis. Contribution of Working Group I to the Sixth
668 Assessment Report of the Intergovernmental Panel on Climate Change, edited by: Masson-Delmotte, V., Zhai, P.,
669 Pirani, A., Connors, S. L., Péan, C., Berger, S., Caud, N., Chen, Y., Goldfarb, L., Gomis, M. I., Huang, M., Leitzell,
670 K., Lonnoy, E., Matthews, J. B. R., Maycock, T. K., Waterfield, T., Yelekçi, Ö., Yu, R., and Zhou, B., Cambridge
671 University Press, Cambridge, United Kingdom and New York, NY, USA,
672 <https://doi.org/10.1017/9781009157896>, 2021.

673 IPCC: Climate Change 2022: Impacts, Adaptation and Vulnerability. Contribution of Working Group II to the
674 Sixth Assessment Report of the Intergovernmental Panel on Climate Change., edited by: Pörtner, H.-O., Roberts,
675 D. C., Tignor, M. M. B., Poloczanska, E. S., Mintenbeck, K., Alegria, A., Craig, M., Langsdorf, S., Löschke, S.,
676 Möller, V., Okem, A., and Rama, B., Cambridge University Press, Cambridge, UK and New York, NY, USA,
677 3056 pp., <https://doi.org/10.1017/9781009325844>, 2022.

678 Ivens, W. P. M. F., Tysmans, D. J. J., Kroeze, C., Löhr, A. J., and van Wijnen, J.: Modeling global N₂O emissions
679 from aquatic systems, *Curr. Opin. Environ. Sustain.*, 3, 350–358, <https://doi.org/10.1016/j.cosust.2011.07.007>,
680 2011.

681 Ji, Q., Frey, C., Sun, X., Jackson, M., Lee, Y.-S., Jayakumar, A., Cornwell, J. C., and Ward, B. B.: Nitrogen and
682 oxygen availabilities control water column nitrous oxide production during seasonal anoxia in the Chesapeake
683 Bay, *Biogeosciences*, 15, 6127–6138, <https://doi.org/10.5194/bg-15-6127-2018>, 2018.

684 Johannsen, A., Dähnke, K., and Emeis, K.: Isotopic composition of nitrate in five German rivers discharging into
685 the North Sea, *Org. Geochem.*, 39, 1678–1689, <https://doi.org/10.1016/j.orggeochem.2008.03.004>, 2008.

686 Kamjunke, N., Rode, M., Baborowski, M., Kunz, J., Zehner, J., Borchardt, D., and Weitere, M.: High irradiation
687 and low discharge promote the dominant role of phytoplankton in riverine nutrient dynamics, *Limnol. Oceanogr.*,
688 66, <https://doi.org/10.1002/lno.11778>, 2021.

689 Kappenberg, J. and Fanger, H.-U.: Sedimenttransportgeschehen in der tidebeeinflussten Elbe, der Deutschen Bucht
690 und in der Nordsee, GKSS-Forschungszentrum, Geesthacht, 2007.

691 Kassambara, A.: ggpubr: “ggplot2” Based Publication Ready Plots, 2023.

692 Kerner, M.: Interactions between local oxygen deficiencies and heterotrophic microbial processes in the elbe
693 estuary, *Limnologica*, 30, 137–143, [https://doi.org/10.1016/S0075-9511\(00\)80008-0](https://doi.org/10.1016/S0075-9511(00)80008-0), 2000.

694 Knowles, R.: Denitrification, *Microbiol. Rev.*, 46, 43–70, <https://doi.org/10.1128/mr.46.1.43-70.1982>, 1982.

695 Koch, M. S., Maltby, E., Oliver, G. A., and Bakker, S. A.: Factors controlling denitrification rates of tidal mudflats
696 and fringing salt marshes in south-west England, *Estuar. Coast. Shelf Sci.*, 34, 471–485,
697 [https://doi.org/10.1016/S0272-7714\(05\)80118-0](https://doi.org/10.1016/S0272-7714(05)80118-0), 1992.

- 698 Kroeze, C., Dumont, E., and Seitzinger, S. P.: New estimates of global emissions of N₂O from rivers and estuaries,
699 *Environ. Sci.*, 2, 159–165, <https://doi.org/10.1080/15693430500384671>, 2005.
- 700 Kroeze, C., Dumont, E., and Seitzinger, S.: Future trends in emissions of N₂O from rivers and estuaries, *J. Integr.*
701 *Environ. Sci.*, 7, 71–78, <https://doi.org/10.1080/1943815X.2010.496789>, 2010.
- 702 Maavara, T., Lauerwald, R., Laruelle, G. G., Akbarzadeh, Z., Bouskill, N. J., Van Cappellen, P., and Regnier, P.:
703 Nitrous oxide emissions from inland waters: Are IPCC estimates too high?, *Glob. Change Biol.*, 25, 473–488,
704 <https://doi.org/10.1111/gcb.14504>, 2019.
- 705 Marzadri, A., Dee, M. M., Tonina, D., Bellin, A., and Tank, J. L.: Role of surface and subsurface processes in
706 scaling N₂O emissions along riverine networks, *Proc. Natl. Acad. Sci.*, 114, 4330–4335,
707 <https://doi.org/10.1073/pnas.1617454114>, 2017.
- 708 Middelburg, J. J. and Herman, P. M. J.: Organic matter processing in tidal estuaries, *Mar. Chem.*, 106, 127–147,
709 <https://doi.org/10.1016/j.marchem.2006.02.007>, 2007.
- 710 Middelburg, J. J. and Nieuwenhuize, J.: Uptake of dissolved inorganic nitrogen in turbid, tidal estuaries, *Mar.*
711 *Ecol.-Prog. Ser.*, 192, 79–88, <https://doi.org/10.3354/meps192079>, 2000.
- 712 Murray, R. H., Erler, D. V., and Eyre, B. D.: Nitrous oxide fluxes in estuarine environments: response to global
713 change, *Glob. Change Biol.*, 21, 3219–3245, <https://doi.org/10.1111/gcb.12923>, 2015.
- 714 Nevison, C., Butler, J. H., and Elkins, J. W.: Global distribution of N₂O and the ΔN₂O-AOU yield in the subsurface
715 ocean, *Glob. Biogeochem. Cycles*, 17, 1119, <https://doi.org/10.1029/2003GB002068>, 2003.
- 716 Nightingale, P. D., Malin, G., Law, C. S., Watson, A. J., Liss, P. S., Liddicoat, M. I., Boutin, J., and Upstill-
717 Goddard, R. C.: In situ evaluation of air-sea gas exchange parameterizations using novel conservative and volatile
718 tracers, *Glob. Biogeochem. Cycles*, 14, 373–387, <https://doi.org/10.1029/1999GB900091>, 2000.
- 719 Nixon, S. W., Ammerman, J. W., Atkinson, L. P., Berounsky, V. M., Billen, G., Boicourt, W. C., Boynton, W. R.,
720 Church, T. M., Ditoro, D. M., Elmgren, R., Garber, J. H., Giblin, A. E., Jahnke, R. A., Owens, N. J. P., Pilson, M.
721 E. Q., and Seitzinger, S. P.: The fate of nitrogen and phosphorus at the land-sea margin of the North Atlantic
722 Ocean, *Biogeochemistry*, 35, 141–180, <https://doi.org/10.1007/BF02179826>, 1996.
- 723 Norbisrath, M., Pätsch, J., Dähnke, K., Sanders, T., Schulz, G., van Beusekom, J. E. E., and Thomas, H.: Metabolic
724 alkalinity release from large port facilities (Hamburg, Germany) and impact on coastal carbon storage,
725 *Biogeosciences*, 19, 5151–5165, <https://doi.org/10.5194/bg-19-5151-2022>, 2022.
- 726 Pätsch, J., Serna, A., Dähnke, K., Schlarbaum, T., Johannsen, A., and Emeis, K.-C.: Nitrogen cycling in the
727 German Bight (SE North Sea) — Clues from modelling stable nitrogen isotopes, *Cont. Shelf Res.*, 30, 203–213,
728 <https://doi.org/10.1016/j.csr.2009.11.003>, 2010.
- 729 Pind, A., Risgaard-Petersen, N., and Revsbech, N. P.: Denitrification and microphytobenthic NO₃⁻ consumption
730 in a Danish lowland stream: diurnal and seasonal variation, *Aquat. Microb. Ecol.*, 12, 275–284,
731 <https://doi.org/10.3354/ame012275>, 1997.
- 732 Quick, A. M., Reeder, W. J., Farrell, T. B., Tonina, D., Feris, K. P., and Benner, S. G.: Nitrous oxide from streams
733 and rivers: A review of primary biogeochemical pathways and environmental variables, *Earth-Sci. Rev.*, 191, 224–
734 262, <https://doi.org/10.1016/j.earscirev.2019.02.021>, 2019.
- 735 Quiel, K., Becker, A., Kirchesch, V., Schöl, A., and Fischer, H.: Influence of global change on phytoplankton and
736 nutrient cycling in the Elbe River, *Reg. Environ. Change*, 11, 405–421, <https://doi.org/10.1007/s10113-010-0152-2>, 2011.
- 738 The R Stats Package, Version 4.0.2:
739 <https://www.rdocumentation.org/packages/stats/versions/3.6.2/topics/prcomp>, last access: 29 January 2021.
- 740 Radach, G. and Pätsch, J.: Variability of continental riverine freshwater and nutrient inputs into the North Sea for
741 the years 1977–2000 and its consequences for the assessment of eutrophication, *Estuaries Coasts*, 30, 66–81,
742 <https://doi.org/10.1007/BF02782968>, 2007.

- 743 Reading, M. J., Tait, D. R., Maher, D. T., Jeffrey, L. C., Looman, A., Holloway, C., Shishaye, H. A., Barron, S.,
744 and Santos, I. R.: Land use drives nitrous oxide dynamics in estuaries on regional and global scales, *Limnol.*
745 *Oceanogr.*, 65, 1903–1920, <https://doi.org/10.1002/lno.11426>, 2020.
- 746 Redfield, A. C., Ketchum, B. H., and Richards, F. A.: The influence of organisms on the composition of sea-water,
747 *Compos. Seawater Comp. Descr. Oceanogr. Sea Ideas Obs. Prog. Study Seas*, 2, 26–77, 1963.
- 748 Rewrie, L. C. V., Voynova, Y. G., van Beusekom, J. E. E., Sanders, T., Körtzinger, A., Brix, H., Ollesch, G., and
749 Baschek, B.: Significant shifts in inorganic carbon and ecosystem state in a temperate estuary (1985 - 2018),
750 *Limnol. Oceanogr.*, submitted.
- 751 Rhee, T. S.: The process of air -water gas exchange and its application, Texas A&M University, College Station,
752 2000.
- 753 Rhee, T. S., Kettle, A. J., and Andreae, M. O.: Methane and nitrous oxide emissions from the ocean: A
754 reassessment using basin-wide observations in the Atlantic, *J. Geophys. Res. Atmospheres*, 114, D12304,
755 <https://doi.org/10.1029/2008JD011662>, 2009.
- 756 Robinson, A. D., Nedwell, D. B., Harrison, R. M., and Ogilvie, B. G.: Hypernutrified estuaries as sources of N₂
757 O emission to the atmosphere: the estuary of the River Colne, Essex, UK, *Mar. Ecol. Prog. Ser.*, 164, 59–71,
758 <https://doi.org/10.3354/meps164059>, 1998.
- 759 Rosamond, M. S., Thuss, S. J., and Schiff, S. L.: Dependence of riverine nitrous oxide emissions on dissolved
760 oxygen levels, *Nat. Geosci.*, 5, 715–718, <https://doi.org/10.1038/ngeo1556>, 2012.
- 761 Rosenhagen, G., Schatzmann, M., and Schrön, A.: Das Klima der Metropolregion auf Grundlage meteorologischer
762 Messungen und Beobachtungen, in: *Klimabericht für die Metropolregion Hamburg*, edited by: von Storch, H. and
763 Claussen, M., Springer, Berlin, Heidelberg, 19–59, https://doi.org/10.1007/978-3-642-16035-6_2, 2011.
- 764 Rosentreter, J. A., Wells, N. S., Ulseth, A. J., and Eyre, B. D.: Divergent Gas Transfer Velocities of CO₂, CH₄,
765 and N₂O Over Spatial and Temporal Gradients in a Subtropical Estuary, *J. Geophys. Res. Biogeosciences*, 126,
766 e2021JG006270, <https://doi.org/10.1029/2021JG006270>, 2021.
- 767 Sanders, T., Schöl, A., and Dähnke, K.: Hot Spots of Nitrification in the Elbe Estuary and Their Impact on Nitrate
768 Regeneration, *Estuaries Coasts*, 41, 128–138, <https://doi.org/10.1007/s12237-017-0264-8>, 2018.
- 769 Scharfe, M., Callies, U., Blöcker, G., Petersen, W., and Schroeder, F.: A simple Lagrangian model to simulate
770 temporal variability of algae in the Elbe River, *Ecol. Model.*, 220, 2173–2186,
771 <https://doi.org/10.1016/j.ecolmodel.2009.04.048>, 2009.
- 772 Schoer, J. H.: Determination of the origin of suspended matter and sediments in the Elbe estuary using natural
773 tracers, *Estuaries*, 13, 161–172, <https://doi.org/10.2307/1351585>, 1990.
- 774 Schöl, A., Hein, B., Wyrwa, J., and Kirchesch, V.: Modelling Water Quality in the Elbe and its Estuary – Large
775 Scale and Long Term Applications with Focus on the Oxygen Budget of the Estuary, *Küste*, 203–232, 2014.
- 776 Schroeder, F.: Water quality in the Elbe estuary: Significance of different processes for the oxygen deficit at
777 Hamburg, *Environ. Model. Assess.*, 2, 73–82, <https://doi.org/10.1023/A:1019032504922>, 1997.
- 778 Sharma, N., Flynn, E. D., Catalano, J. G., and Giammar, D. E.: Copper availability governs nitrous oxide
779 accumulation in wetland soils and stream sediments, *Geochim. Cosmochim. Acta*, 327, 96–115,
780 <https://doi.org/10.1016/j.gca.2022.04.019>, 2022.
- 781 Siedler, G. and Peters, H.: Properties of sea water, Physical properties, in: *Oceanography*, vol. V/3a, edited by:
782 Sündermann, J., Springer, Berlin, Germany, 233–264, 1986.
- 783 Silvennoinen, H., Hietanen, S., Liikanen, A., Stange, C. F., Russow, R., Kuparinen, J., and Martikainen, P. J.:
784 Denitrification in the River Estuaries of the Northern Baltic Sea, *AMBIO J. Hum. Environ.*, 36, 134–140,
785 [https://doi.org/10.1579/0044-7447\(2007\)36\[134:DITREO\]2.0.CO;2](https://doi.org/10.1579/0044-7447(2007)36[134:DITREO]2.0.CO;2), 2007.

786 Smith, R. L. and Böhlke, J. K.: Methane and nitrous oxide temporal and spatial variability in two midwestern USA
787 streams containing high nitrate concentrations, *Sci. Total Environ.*, 685, 574–588,
788 <https://doi.org/10.1016/j.scitotenv.2019.05.374>, 2019.

789 Sommerfield, C. K. and Wong, K.-C.: Mechanisms of sediment flux and turbidity maintenance in the Delaware
790 Estuary, *J. Geophys. Res. Oceans*, 116, C01005, <https://doi.org/10.1029/2010JC006462>, 2011.

791 Tang, W., Tracey, J. C., Carroll, J., Wallace, E., Lee, J. A., Nathan, L., Sun, X., Jayakumar, A., and Ward, B. B.:
792 Nitrous oxide production in the Chesapeake Bay, *Limnol. Oceanogr.*, 67, 2101–2116,
793 <https://doi.org/10.1002/lno.12191>, 2022.

794 Tian, H., Xu, R., Canadell, J. G., Thompson, R. L., Winiwarter, W., Suntharalingam, P., Davidson, E. A., Ciais,
795 P., Jackson, R. B., Janssens-Maenhout, G., Prather, M. J., Regnier, P., Pan, N., Pan, S., Peters, G. P., Shi, H.,
796 Tubiello, F. N., Zaehle, S., Zhou, F., Arneeth, A., Battaglia, G., Berthet, S., Bopp, L., Bouwman, A. F., Buitenhuis,
797 E. T., Chang, J., Chipperfield, M. P., Dangal, S. R. S., Dlugokencky, E., Elkins, J. W., Eyre, B. D., Fu, B., Hall,
798 B., Ito, A., Joos, F., Krummel, P. B., Landolfi, A., Laruelle, G. G., Lauerwald, R., Li, W., Lienert, S., Maavara,
799 T., MacLeod, M., Millet, D. B., Olin, S., Patra, P. K., Prinn, R. G., Raymond, P. A., Ruiz, D. J., van der Werf, G.
800 R., Vuichard, N., Wang, J., Weiss, R. F., Wells, K. C., Wilson, C., Yang, J., and Yao, Y.: A comprehensive
801 quantification of global nitrous oxide sources and sinks, *Nature*, 586, 248–256, <https://doi.org/10.1038/s41586-020-2780-0>, 2020.

803 US EPA: Volunteer Estuary Monitoring: A Methods Manual, United States Environmental Protection Agency
804 (EPA), 2006.

805 Walter, S., Bange, H. W., and Wallace, D. W. R.: Nitrous oxide in the surface layer of the tropical North Atlantic
806 Ocean along a west to east transect, *Geophys. Res. Lett.*, 31, L23S07, <https://doi.org/10.1029/2004GL019937>,
807 2004.

808 Wanninkhof, R.: Relationship between wind speed and gas exchange over the ocean, *J. Geophys. Res. Oceans*, 97,
809 7373–7382, <https://doi.org/10.1029/92JC00188>, 1992.

810 Weiss, R. F.: The solubility of nitrogen, oxygen and argon in water and seawater, *Deep Sea Res. Oceanogr. Abstr.*,
811 17, 721–735, [https://doi.org/10.1016/0011-7471\(70\)90037-9](https://doi.org/10.1016/0011-7471(70)90037-9), 1970.

812 Weiss, R. F. and Price, B. A.: Nitrous oxide solubility in water and seawater, *Mar. Chem.*, 8, 347–359,
813 [https://doi.org/10.1016/0304-4203\(80\)90024-9](https://doi.org/10.1016/0304-4203(80)90024-9), 1980.

814 Wells, N. S., Maher, D. T., Erler, D. V., Hipsey, M., Rosentreter, J. A., and Eyre, B. D.: Estuaries as Sources and
815 Sinks of N₂O Across a Land Use Gradient in Subtropical Australia, *Glob. Biogeochem. Cycles*, 32, 877–894,
816 <https://doi.org/10.1029/2017GB005826>, 2018.

817 Wertz, S., Goyer, C., Burton, D. L., Zebarth, B. J., and Chantigny, M. H.: Processes contributing to nitrite
818 accumulation and concomitant N₂O emissions in frozen soils, *Soil Biol. Biochem.*, 126, 31–39,
819 <https://doi.org/10.1016/j.soilbio.2018.08.001>, 2018.

820 de Wilde, H. P. and de Bie, M. J.: Nitrous oxide in the Schelde estuary: production by nitrification and emission
821 to the atmosphere, *Mar. Chem.*, 69, 203–216, [https://doi.org/10.1016/S0304-4203\(99\)00106-1](https://doi.org/10.1016/S0304-4203(99)00106-1), 2000.

822 Winterwerp, J. C. and Wang, Z. B.: Man-induced regime shifts in small estuaries—I: theory, *Ocean Dyn.*, 63,
823 1279–1292, <https://doi.org/10.1007/s10236-013-0662-9>, 2013.

824 WMO: Scientific Assessment of Ozone Depletion: 2018, World Meteorological Organization, Geneva,
825 Switzerland, 2018.

826 Wolfstein, K. and Kies, L.: Composition of suspended particulate matter in the Elbe estuary: Implications for
827 biological and transportation processes, *Dtsch. Hydrogr. Z.*, 51, 453–463, <https://doi.org/10.1007/BF02764166>,
828 1999.

829 Wrage, N., Velthof, G. L., van Beusichem, M. L., and Oenema, O.: The role of nitrifier denitrification in the
830 production of nitrous oxide, *Soil Biol. Biochem.*, 33, 1723–1732, [https://doi.org/10.1016/S0038-0717\(01\)00096-7](https://doi.org/10.1016/S0038-0717(01)00096-7),
831 2001.

- 832 Yevenes, M. A., Bello, E., Sanhueza-Guevara, S., and Farías, L.: Spatial Distribution of Nitrous Oxide (N₂O) in
833 the Reloncaví Estuary–Sound and Adjacent Sea (41°–43° S), Chilean Patagonia, *Estuaries Coasts*, 40, 807–821,
834 <https://doi.org/10.1007/s12237-016-0184-z>, 2017.
- 835 Zander, F., Heimovaara, T., and Gebert, J.: Spatial variability of organic matter degradability in tidal Elbe
836 sediments, *J. Soils Sediments*, 20, 2573–2587, <https://doi.org/10.1007/s11368-020-02569-4>, 2020.
- 837 Zander, F., Groengroeft, A., Eschenbach, A., Heimovaara, T. J., and Gebert, J.: Organic matter pools in sediments
838 of the tidal Elbe river, *Limnologica*, 96, 125997, <https://doi.org/10.1016/j.limno.2022.125997>, 2022.
- 839 ZDM: Abfluss - Neu Darchau, edited by: Wasserstraßen- und Schifffahrtsamt Elbe, 2022.